2017-01-01

Characterizing Regulatory Factors Of The Sumoylation System

David Quintanar
University of Texas at El Paso, dquintanar@miners.utep.edu

CHARACTERIZING REGULATORY FACTORS OF THE SUMOYLATION SYSTEM

DAVID QUINTANAR

Master's Program in Biological Sciences

APPROVED:

German Rosas-Acosta, Ph.D., Chair

Giulio Francia, Ph.D.

Delfina Dominguez, Ph.D.

Charles Ambler, Ph.D.
Dean of the Graduate School

CHARACTERIZING REGULATORY FACTORS OF THE SUMOYLATION SYSTEM

by

DAVID QUINTANAR

THESIS DEFENSE

Presented to the Faculty of the Graduate School of
The University of Texas at El Paso
in Partial Fulfillment
of the Requirements
for the Degree of

MASTER OF SCIENCE

Department of Biological Sciences
THE UNIVERSITY OF TEXAS AT EL PASO
May 2017

Abstract

The effects that influenza's seasonal epidemics have on human health and the global economy have been clearly noted; while they are indeed very impressive, the impact of influenza pandemics arguably surpass other known infectious agents. Influenza A virus attaches to, enters, and infect cells by releasing its segmented genome which localize to the nucleus then use the host's cellular machinery to replicate and create viral progeny. The virus is able to hijack transcriptional components as well as to interact with other known and unknown host proteins which ultimately allows for a balance between cell viability and viral propagation. One known system that is required for the viral life cycle is the SUMOylation system. Several influenza A viral proteins need to be SUMOylated to function properly. Our lab was the first to show that proteins from influenza A are SUMOylated in a tissue culture model. This was followed by verification, by ours and other groups, that non-SUMOylatable forms of the same viral proteins resulted in loss of function or diminished viral propagation. The Non Structural protein 1 (NS1) is known for its role as an immune response antagonist. NS1 is also a protein that requires SUMOylation to function properly. Rather than target viral components which easily overcome current therapeutics with single point mutations, understanding and then modulating the SUMOylation system to impede viral replication may be a viable alternative to combat influenza. The SUMOylation system has been tied to both the immune and the cellular stress response systems. Regulation of the SUMOylation system, however, is not yet fully understood. The aim of this study is to characterize potential regulatory factors of the SUMOylation system which could in turn have a downstream effect on the cellular stress and immune response. This will be accomplished by using several models which are known to induce an increase in the SUMO profile; both expression levels of SUMO as well as its conjugation to target proteins. The first aim of this project is to optimize all protocols needed to induce increases in SUMOylation using three models; heat shock, hypoxia, and influenza infection. The second part of Aim 1 will lead to the standardization of protocols to

determine if the changes in SUMO expression and conjugation is regulated at the transcriptional level. Quantitative Reverse Transcriptase - Polymerase Chain Reaction (qRT-PCR) will be used to measure SUMO1 transcript levels after treating cells with several factors known to induce SUMOylation increases, e.g. Infection, heat shock, and hypoxia.

The second aim of this project, to further understand how SUMO is regulated, will be to optimize the steps required to conduct an efficient and fully reproducible proteomic analysis of SUMO modified proteins. Collection of the samples requires standardized procedures that minimize loss and contamination of the sample. Quality control measures are included in order to avoid degradation and inaccuracy. The differentially SUMOylated proteins, after infection, may be key players involved in the immune response regardless if SUMOylation activates or inhibits them. Antibodies against SUMO1 will allow for the isolation and enrichment of the SUMO modified proteins in the most non-artificial biologically accurate setting. Proteins which interact with SUMO before and after treatment will be compared after analysis by Tandem Liquid Chromatography Mass Spectrometry (LC-MS/MS). To perform this analysis a large amount of antibodies will be required. Liquid tumors, known as ascites, are able to form in mice when inoculated by fusion cells. These hybridoma cells are comprised of b-cells fused with myeloma cells. These cells can be grown in animal cavities until large volumes of ascitic fluid, with a high concentration of antibodies, are later extracted and sold commercially. Optimization of this technique is a major focus of my second aim.

Table of Contents

List of Tables

List of Figures

Chapter 1: General Introduction

1.1 THE GLOBAL IMPACT OF INFLUENZA

Influenza virus causes seasonal epidemics resulting in significant morbidity and mortality, primarily in the very young and the elderly [Mubareka et al. 2013]. Infection by influenza for individuals over the age of sixty-five results in increased mortality when compared to other respiratory viruses [Thompson et al. 2003]. Seasonal epidemics cause close to 500,000 deaths worldwide annually, ten percent occurring in the United States [Pillet et al. 2011; Maines et al. 2012]. New virulent strains of influenza, to which pre-existing immunity in the global population is not present, emerge at unpredictable periodicity and result in high mortality and morbidity [Rewar, Mirdha, & Rewar, 2015]. These outbreaks lead to global pandemics, and have claimed the lives of over 100 million people in the last century, independent of their age or health status [Mubareka et al. 2013]. Four pandemics have occurred in the last one hundred years, with the 1918 "Spanish Flu" claiming the lives of an estimated 50 million people [Johnson & Mueller, 2002]. Seasonal epidemics as well as the less frequent global pandemics have severe consequences for both human health and the global economy. Transmission and reassortment studies have demonstrated that the 2009 H1N1 pandemic strain of swine origin has the potential to undergo reassortment with the highly pathogenic H5N1 avian influenza virus if coinfection in a susceptible host occurs [Octaviani et al. 2010; Tao, Li, White, Steel, & Lowen, 2015]. Both of these strains are currently circulating in human and animal reservoirs and this recombination would allow the extremely virulent H5N1 avian strain (with a mortality rate above 60%) to become highly transmissible among humans. This would potentially result in one of the deadliest pandemics to date [Octaviani et al. 2010]. Several emerging strains of influenza have been shown to contain mutations in surface proteins that allow for complete evasion of current antiviral treatments [Kageyama et al. 2013)]. The majority of human strains of influenza, including pandemic 2009 H1N1, are resistant to the adamantane M2 ion channel inhibitors [Watanabe et al. 2010]. IAV

resistance to neuraminidase inhibitors, such as oseltamivir, is occurring at higher frequencies and this highlights the flaw with targeting poorly conserved viral components [Watanabe et al. 2010]. The limitations of current therapeutics to diminish the spread of influenza as well as the threat of a pandemic support the urgent need for research aimed at developing novel therapeutics against Influenza A virus. In order to address influenza epidemics through the development of therapeutics which inhibit viral transmissibility as well as propagation, more research is required. A better understanding of both how viral components interact with the host system and how the host cellular system regulates immune responses is needed to develop more effective methods to combat influenza.

1.2 THE INFLUENZA A VIRUS

Influenza A is a negative-sense single stranded RNA virus from the family *Orthomyxoviridae* [Edinger, Pohl, & Stertz, 2014]. The host derived lipid-enveloped virus contains eight genome segments which encode at least 11 viral proteins [Steinhauer & Skehel, 2002; Watanabe et al. 2010]. Influenza can be further classified into subtypes based on variations in its surface glycoproteins which govern the viral lifecycle at cellular entry and release of virions, hemagglutinin (HA) and neuraminidase (NA) [Bender et al. 1999]. There are currently 18 hemagglutinin and 10 neuraminidase variants which allow for hundreds of viral subtype combinations; this high variability is another example of how targeting viral components for therapeutics is not ideal [Gamblin & Skehel, 2010; Tong et al. 2012; 2013]. The nomenclature assigned to influenza viruses detail key information about the strain. Virus type (A), species of origin unless human, location isolated (Panama), isolate number (2007), and year of isolation (1999) are listed in that order - **A/Panama/2007/1999(H3N2).** Human strains do not specify human as the species of origin but include the hemagglutinin and neuraminidase subtypes [Bouvier & Palese, 2008; Cinti, 2005]. Subtypes of influenza are labeled by their surface protein variants, as exemplified by the denominations “H1N1” swine flu or “H5N1” avian flu. The majority of viral

subtypes are classified, based on their virulence in chickens, as Low Pathogenic Avian Influenza (LPAI) viruses or Highly Pathogenic Avian Influenza (HPAI) [Herfst, Schrauwen et al. 2012]. After reassortment, influenza A viruses of the H5 and H7 subtypes can give rise to strains of Highly Pathogenic Avian Influenza (HPAI) [Herfst, Schrauwen et al. 2012].

1.3 INFLUENZA VIRAL COMPONENTS

Influenza A viruses have an RNA genome consisting of eight gene segments associated to four viral proteins to form the viral ribonucleoprotein complex (vRNP) [Herfst, Schrauwen et al. 2012]. This relatively simple structure enables the virus to manipulate the host cellular machinery to its advantage by either enhancing or inhibiting certain cell functions during each step of the viral life cycle. Segments one, two, and three encode three of the four proteins that are needed to form this complex: basic polymerase 2 (PB2), basic polymerase 1 (PB1), and acidic polymerase (PA), respectively (see table 1). The fourth protein needed to form the vRNP, nucleocapsid protein (NP), coats the viral RNA and is encoded by the fifth genome segment [Herfst, Schrauwen et al. 2012]. These four proteins are involved in viral genome transcription and replication and are referred to as the viral RNA dependent RNA polymerase (vRdRp) [Herfst, Schrauwen et al. 2012]. In some viral strains, the second genome segment has also been shown to encode a second small protein, PB1-F2, which has been implicated in the induction of cell death [Chen et al. 2001].

The structure of influenza virus is dependent on four viral proteins. Two of the four surface transmembrane proteins HA and NA are embedded into the lipid envelope and are encoded by segments four and six, respectively [Shaw, Stone et al. 2008]. Hemagglutinin i) binds to sialic acids on the host cell surface for viral docking, allowing for entry via endocytosis, and ii) is required for fusion between the virus and late endosome membranes [Herfst, Schrauwen et al. 2012]. Neuraminidase is a viral enzyme responsible for cleaving sialic acids, releasing progeny virions from the host cell surface to continue the infection cycle [Herfst, Schrauwen et al. 2012; Watanabe et al. 2010].

Segment seven encodes for the third and fourth structural proteins, M1 and M2 [Herfst, Schrauwen et al. 2012]. M2 ion channel protein is also a transmembrane protein, present at lower levels than the other surface proteins, which delivers protons from the late endosome into the virus interior [Shen, Lou, & Wang, 2015]. This acidification triggers the change in hemagglutinin that allows for virus-host membrane fusion and vRNP release [Shen, Lou, & Wang, 2015]. M1 is the viral matrix protein which lines the inner surface of the virion, supporting its structure and acting as binding site for the vRNPs required for packaging [Herfst, Schrauwen et al. 2012].

The last viral genome segment encodes for two non-structural proteins NS1 (non-structural protein 1) and the NEP (nuclear-export protein) previously known as NS2 [Herfst, Schrauwen et al. 2012]. NS1 is the main viral antagonist of cellular innate immune responses, whereas NEP, which is encoded by a spliced product of the NS1 segment, is involved in the nuclear export of vRNPs into the cytoplasm before virus assembly [Herfst, Schrauwen et al. 2012]. A new strain of influenza, carrying an NS gene segment coding for a non-SUMOylatable form of NS1, was created utilizing the 12 plasmid reverse genetics system previously described [Santos et al. 2013]. This strain, referred to as WNS/T7T7[NS1K70AK219A~NS2] will be included in this analysis to test if the changes in the expression of SUMO1 transcripts, SUMO conjugation, and viral life cycle are dependent on the SUMOylation of NS1.

Table 1.1 Proteins encoded by viral RNA segments.

The negative sense single-stranded RNA of the influenza A genome is packaged into eight ribonucleoprotein (RNP) complexes. A minimum of 11 proteins are encoded by almost all strains of influenza [Steinhauer & Skehel, 2002].

RNA Segment	Viral Protein	Function	Gene Size (bp)
1	PB2	Basic polymerase 2; polymerase component; host cap binding	2341
2	PB1	Basic polymerase 1; polymerase component; catalytic subunit	2341
	PB1-F2	Apoptosis induction; interferon antagonist; modulate polymerase activity	
3	PA	Acidic polymerase; cap snatching endonuclease; replication of viral genome	2233
4	HA	Hemagglutinin; antigenic determinant; surface glycoprotein; binds host receptors on cell membrane; fusion with endosomal membrane	1778
5	NP	Nucleoprotein; viral ribonucleoprotein (vRNP) complex component; viral assembly; RNA synthesis	1565
6	NA	Neuraminidase; antigenic determinant; surface glycoprotein; release of new viral particles by cleaving sialic acids	1413
7	M1	Matrix protein; viral assembly	1027
	M2	Transmembrane ion-channel; viral disassembly upon infection	
8	NS1	Non-structural protein; interferon antagonist; suppresses host gene expression; modulates mRNA splicing and translation	890
	NEP	Nuclear export protein; trafficking of vRNPs for viral assembly	

1.4 INFLUENZA INFECTION AND LIFECYCLE

Unlike most RNA viruses, IAV replicates in the nucleus. Therefore, the virus has to overcome several barriers on its way to the site of replication and, simultaneously, avoid being recognized by the innate immune system. The viral lifecycle is a dynamic process that requires the completion of several distinct steps: attachment to target cells (I), internalization by receptor mediated endocytosis (II), membrane fusion between the virus envelope and the endosome which leads to the uncoating and release of vRNPs into the cytoplasm (III), nuclear localization of the vRNPs using import machinery of the host cell nuclear pore complex (IV), two stage replication (V), nuclear export, processing, assembly and release (VI) (**Fig. 1**). During this process, influenza uses many host cellular functions and a more complete understanding of how these mechanisms are regulated will help in the development of novel therapeutics by allowing researchers to target key interactions needed for viral propagation and the host immune response.

Reassortment between strains from different host reservoirs allows for new and virulent, pandemic rated strains to arise; this may have severe consequences for the human population [Edinger, Pohl, & Stertz, 2014]. The H1N1 swine origin pandemic strain is an example of a strain which crossed over from animals to humans with devastating effects. The attachment and entry process of influenza has been a major target of focus for current antiviral strategies as blocking HA functionality (i.e., sialic acid binding or membrane fusion) should inhibit viral entry, replication, and propagation. However, antibodies developed against either the active site or the stalk of HA have failed to provide the anticipated results.

1.4.1 Viral attachment

The hemagglutinin protein (HA) is a multifunctional viral protein that mediates attachment and fusion to the host cell [Palese & Shaw, 2007]. HA is initially synthesized as a single polypeptide precursor (HA0), which is cleaved into the HA1 and HA2 subunits by trypsin-like

proteases in the host cell [Horimoto & Kawaoka, 2005; Galloway et al., 2013]. The switch from LPAI to HPAI virus phenotypes occurs upon the introduction of several basic amino acid residues into the HA0 cleavage site, also known as the multi basic cleavage site (MBCS) (see figure 1) [Horimoto & Kawaoka, 2005]. HA sequence dependent cleavage has been shown to be a determining factor for infection and pathogenicity [Horimoto & Kawaoka, 2005]. HA's of LPAI viruses have a short arginine cleavage site (**R**ET**R**) and can only be cleaved by respiratory and intestinal proteases, while HA's of HPAI viruses contain multiple basic amino acids in their cleavage site (**R**E**RRRKKR**) and can be cleaved by a number of proteases in a wide range of organs [Horimoto & Kawaoka, 2005]. Infection with this type of virus can become systemic with lethal effects. Upon cleavage, the HA protein, expressed as a trimer, interacts with the host N-acetylneuraminic acid (sialic acid) through its receptor binding pocket (RBP) [Bouvier & Palese, 2008; Edinger, Pohl, & Stertz, 2014]. Sialic acid residues are found at the outer ends of N- and O-linked glycoproteins or lipids and interact with the underlying sugar, galactose, via an α2,3 or α2,6 linkage [Ito et al. 1998; Matrosovich et al. 2000]. The second carbon atom of the sialic acid is bound to either the third or sixth carbon of the galactose, respectively, by an oxygen atom [Ito et al. 1998; Matrosovich et al. 2000]. Avian strains of influenza are able to interact most efficiently with sialic acids in the α2,3 configuration, mostly found in waterfowl epithelia [Ito et al. 1998; Matrosovich et al. 2000]. In contrast, human strains of influenza exhibit preferential binding to sialic acids in the α2,6 configuration, which is the predominant type found in human epithelia [Ito et al. 1998; Matrosovich et al. 2000]. Alpha 2,3 linked sialic acids are found in humans, however, in lower numbers, mostly on ciliated epithelial cells, and lower in the respiratory tract [Ito et al. 1998; Matrosovich et al. 2000]. Strains of IAV that are highly transmissible between humans require the ability to bind to α2,6 linkages as seen in several pandemics (1918 "Spanish Flu") [Ito et al. 1998; Matrosovich et al. 2000; Davis et al. 2016]. Swine trachea contain both types of sialic acid interactions and could serve as a "reassortment vessel" leading to the emergence of new viruses, as exemplified by the H1N1 swine flu which contains segments from all three hosts -

avian, swine, and human [Nelson & Vincent, 2015]. The sialic acid interacting site, RBP, is located at the globular end of the HA trimer, is highly conserved among HA subtypes, and acts as the primary contact site between the virus and the host cell [Weis et al. 1988; Edinger, Pohl, & Stertz, 2014]. Because the HA to sialic acid is a low affinity interaction, multiple interactions must take place to strengthen this attachment [Sauter et al. 1989; Edinger, Pohl, & Stertz, 2014]. HA binding to sialic acids of α2,6 linkage is shown to be dependent on the long umbrella-shaped structure that is a result of this link, while α2,3 have a shorter cone like structure [Chandrasekaran et al. 2008; Edinger, Pohl, & Stertz, 2014]. Upon attachment, influenza is then able to enter host cells and systematically reprogram the cellular environment to its advantage.

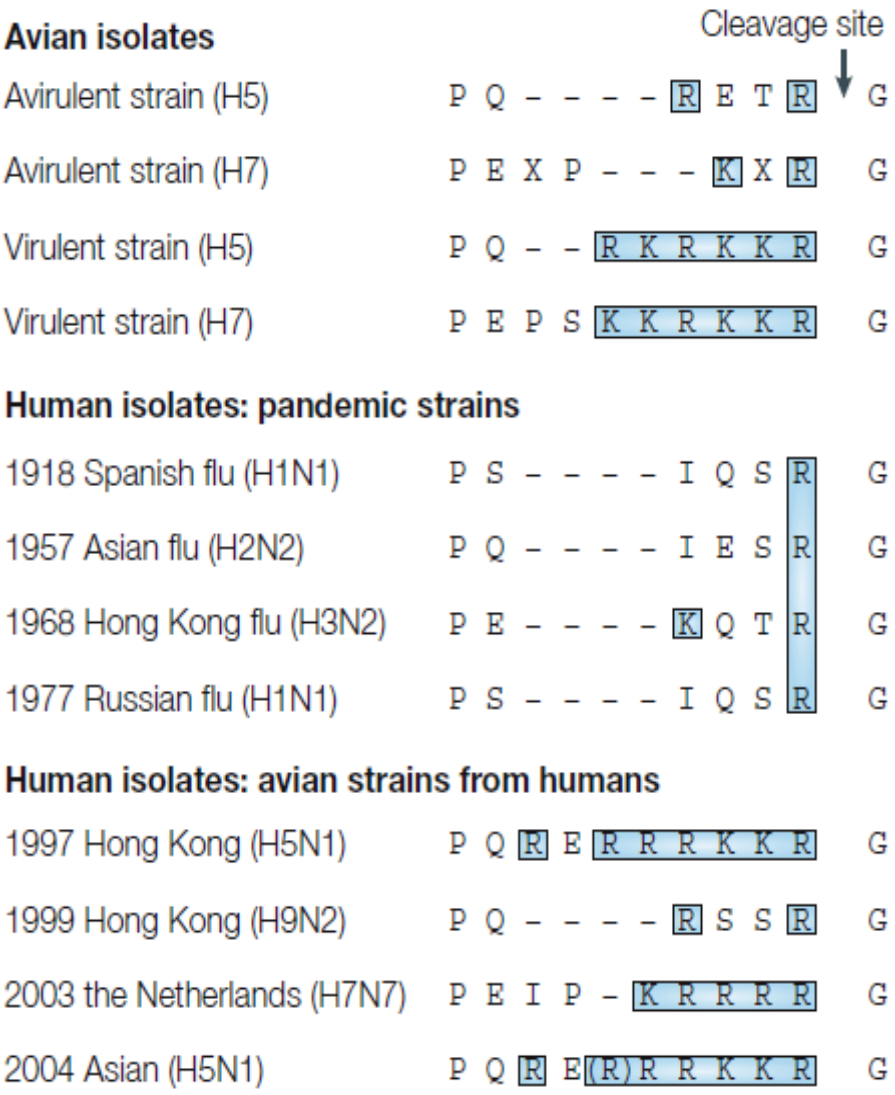

Figure 1.1 Multi Basic Cleavage Site.

HA cleavage site sequence of influenza A viruses. Basic amino acids are shown in blue boxes. Virulent strains have multiple arginine and lysine residues. Dashes are for the purpose of alignment only.

Image from Horimoto, T., & Kawaoka, Y. (2005). Influenza: lessons from past pandemics, warnings from current incidents. Nature Reviews. Microbiology, 3(8), 591–600. http://doi.org/10.1038/nrmicro1208.

1.4.2 Endosome trafficking, membrane fusion, and uncoating

Upon receptor binding, internalization of the viral particle into the host cell is able to occur. Internalization can be mediated by clathrin-dependent endocytosis (spherical virions) but also by non clathrin-dependent pathways; e.g. macropinocytosis (filamentous virions) [Mercer & Helenius, 2012; Watanabe et al. 2010; Chan et al. 2016; Chlanda & Zimmerberg, 2016]. Influenza internalization, but not attachment, has recently been shown to be heavily dependent on the abundantly expressed Nucleolin (NCL) protein which is implicated in a large number of cellular activities [Chan et al. 2016]. NCL is known to localize to the nucleoplasm, cytoplasm, as well as the cell surface and has been described to play a role is several important life cycle stages for multiple viruses [Greco et al. 2012; Tayyari et al. 2011; Chan, et al. 2016]. The main route for viral entry, clathrin dependent endocytosis, is facilitated by recruitment of the clathrin adaptor protein Epsin-1 to the host side of the viral binding site [Chen & Zhuang, 2008]. The resulting endosome undergoes pH changes at early and later stages of endocytosis. In the early endosome, the proton pump induced acidification causes a conformational change in HA but it is not until the late endosome reaches a pH of 5 that membrane fusion is achieved [Grove & Marsh, 2011; White & Whittaker, 2016]. The fusion of the viral envelope and the cellular endosome is mediated by the hemagglutinin fusion peptide (HAfp) on the N-terminal fragment of the HA2 subunit [Worch, 2014]. The drop in pH triggers the conformational change in HA2 that results in the insertion of the HAfp into the endosomal membrane; the transmembrane domain (TMD) of HA2 is anchored to the viral envelope while the fp domain is now anchored to the endosomal membrane [Cross et al. 2009; Worch, 2014]. During a second conformational change, the HA protein folds, bringing its two ends together resulting in fusion of the two membranes [Luo, 2011]. Disrupting progression from the early to the late endosome by modifying proteins known to regulate intracellular vesicle trafficking halts the viral lifecycle [Watanabe et al. 2010]. More recently, cathepsin W (CtsW), from a superfamily of cysteine proteases involved in numerous cellular functions (apoptosis and inflammatory processes), has been shown to be crucial for viral particle escape from the late

endosome [Edinger et al. 2015]. The internal acidification of the virion is dictated by the M2 ion channel and triggers disassembly of the M1 layer and vRNP release; membrane fusion dependence on pH varies by ~0.7 pH units between influenza strains [White & Whittaker, 2016; Galloway et al. 2013]. Human influenza viruses generally require a lower pH than avian strains but acidification ultimately leads to an expansion of the fusion pore and the release of the vRNPs into the cytoplasm where further subversion of host machinery results in their nuclear import [Chlanda & Zimmerberg, 2016; Galloway et al. 2013; Watanabe et al. 2010].

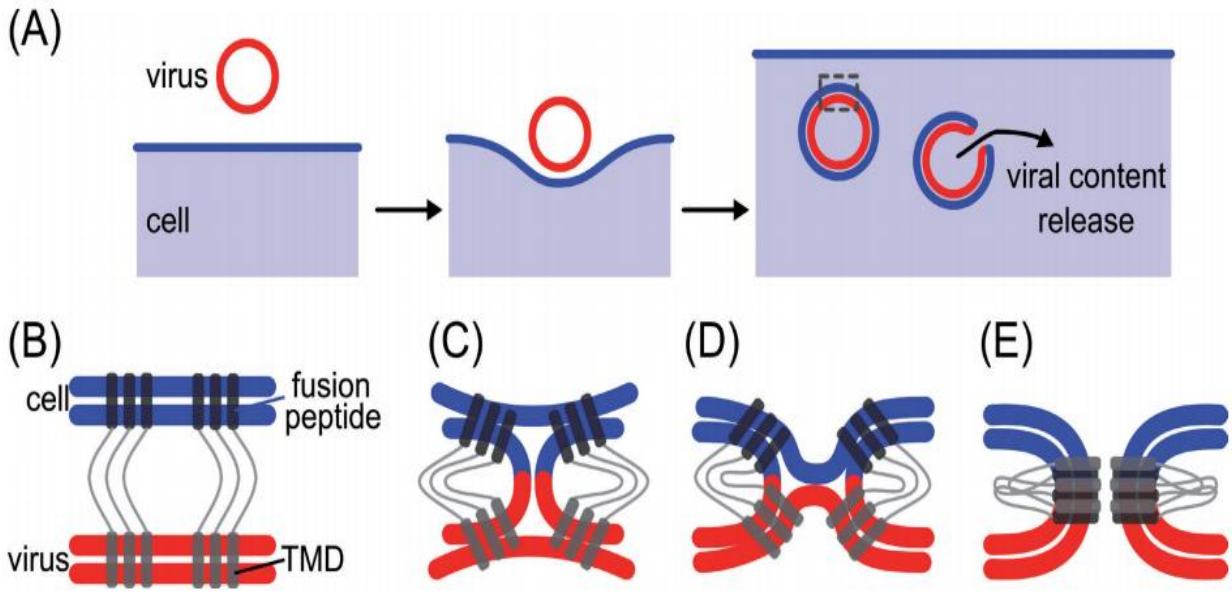

Figure 1.2 Membrane Fusion by HA.
After endocytosis, membrane fusion is depicted in steps B through E. (B) upon the endosome induced drop in pH, the hemagglutinin subunit HA2 which is embedded in the viral envelope by

its TMD then anchors its fusion peptide domain into the inner endosomal membrane. (C) and (D) show the conformational change in HA that result in the contact and fusion of the two distinct membranes. This process results in the formation of the so-called fusion pore (E).

Image from Worch, R. (2014). Structural biology of the influenza virus fusion peptide. Acta Biochim Polonica, 61(3), 421-426.

1.4.3 Nuclear localization, cap-snatching, and mRNA synthesis

Influenza A virus replication, unlike other RNA viruses, takes place in the nucleus and all viral components released in the uncoating step, detailed above, require transport through the nuclear pore complex (NPC) [O'Neil et. al., 1995]. The viral genome and associated proteins utilize a signal based nuclear import mechanism, nuclear localization signals (NLS), to gain entry into the nucleus [Cohen, Au, & Panté, 2011; Wu et. al., 2007]. Each of the separately packed vRNPs has a diameter of approximately 15nm, a length between 50 and 100nm [Compans, Content, & Duesberg, 1972], and are each comprised of a single copy of the trimeric viral RNA polymerase (PB1, PB2, and PA) with several copies of the structural nucleoprotein (NP) [Cohen, Au, & Panté, 2011]. Importin α, a member of the cellular karyopherin import pathway, recognizes cargo proteins containing nuclear localization signals (NLS) and then binds to importin β; the resulting complex - cargo/importin α/β is then transported into the nucleus through the NPC [Wu et. al., 2007]. Influenza vRNPs (PB1, PB2, PA, and NP) contain NLSs and have all been shown to interact with RanBP5 (importin 5), importin α1, as well as importin α2 [Watanabe et. al., 2010; Cohen, Au, & Panté, 2011]. NP contains two characterized NLSs: the more potent mediator of nuclear import, NLS1 which spans residues 1-13 and NLS2 (198-216) which has been shown to be positioned in an RNA binding groove and is less accessible [Cohen, Au, & Panté, 2011; Ye, Krug, & Tao, 2006]. PB1 was also shown to directly interact with RanBP5 via the first 290 N-terminal residues of the polymerase [Hutchinson et. al., 2011]. Import of the vRNPs into the nucleus is followed by viral polymerase activation.

The viral proteins, PB1, PB2, and PA, are major components of the virus each with a distinct function and have a combined mass of ~250 kDa [Das et al., 2010]. This polymerase complex is needed for viral genome transcription and replication. Increased transmissibility and pathogenicity have been tied to an increase in polymerase activity [Naffakh et al., 2008]. Synthesis of viral mRNA requires the binding of PB2, through residues 318-482, to the 5' cap (m7GTP) of host pre-mRNAs. This is followed by a phosphodiester bond cleavage of the nascent mRNA 10-

13 nucleotides downstream of the cap, facilitated by the endonuclease domain at the N-terminus of PA – a process known as "cap snatching" [Das et. al., 2010; Dias et al., 2009; Yuan et al., 2009; Ulmanen, Broni, & Krug, 1981]. Transcription of the viral mRNA uses the cleaved 3' end of the capped segment as a primer for PB1 binding, which contains enzymatic motifs that allow it to function as a polymerase, and results in the production of viral mRNAs virtually indistinguishable from host mRNAs [reviewed in Das et. al., 2010].

Influenza viral RNAs have a specific structure; i) a long central antisense open-reading frame ii) flanked on each end by two short untranslated regions (UTRs) [Fournier, et al., 2012]. iii) The UTRs contain two partially complementary terminal promoters which are conserved between segments and allow for the panhandle structure to be formed; 13 and 12 nucleotides at the 5' and 3' termini, respectively [Fournier, et al., 2012; Ozawaa & Kawaoka, 2011]. These sequences contain promoter elements recognized by the heterotrimeric RNA-dependent RNA polymerase (RdRp comprised of PB1, PB2, and PA) and are needed for transcription and replication [Fournier, et al., 2012; Ozawaa & Kawaoka, 2011]. The mRNA is used for translation of viral proteins and the cRNAs produced by PB1 serve as the template for the synthesis of vRNA to be packaged in progeny virions [Scull & Rice, 2010].

1.4.4 Two stage lifecycle

Transcription of the viral genome takes place in two stages, early and late. In the nucleus, each vRNP acts as an independent unit for transcription initiating synthesis of 5' capped and 3' polyadenylated viral mRNA which are shuttled out of the nucleus into the cytoplasm for translation; the production of viral proteins necessary for replication utilizes host mechanisms and comprises the first round of viral protein synthesis [reviewed in Santos, Chacón & Rosas-Acosta, 2013; Fodor, 2013; Das et al., 2010]. The 5' cap and the 3' polyadenylated tail ensure that viral mRNA is indistinguishable from host RNA; resulting in nuclear export, protection from degradation, and proper translation [Kapp & Lorsch, 2004]. The proteins expressed in the early

stage of the viral lifecycle are the polymerase proteins, NP, and the non-structural protein NS1 [Palese & Shaw, 2007]. NS1 and PB1-F2 have been shown to be key inhibitors of the cellular antiviral response [Krug et al., 2003; Dudek et al., 2011]. Influenza virus infection shuts off host protein synthesis, thereby enhancing translation of viral mRNAs [Chen & Krug, 2000]. In the second or late stage of viral infection, the proteins synthesized during the early phase localize back into the nucleus and initiate the transcription of late viral genes, which code for structural and surface proteins. The late viral proteins HA, NA, M2, and M1 are sent through the secretory pathway to undergo processing, glycosylation and are localized to the cell membrane [Das et al., 2010]. Later during infection and independent of a primer, the viral polymerase switches from transcription to the replication of vRNA to generate progeny virions. To this end, the RdRp first synthesizes complementary RNA (cRNA), which serves as template, and then synthesizes vRNA, which is coated by NP at an approximate proportion of one NP molecule for every 24 nucleotides [Fodor, 2013; Scull & Rice, 2010]. The ends of each viral mRNA contain signals required for the proper packaging of each genomic segment into the virion through interactions with viral proteins NEP and M1 [reviewed in Fodor, 2013; Neumann, 2000].

1.4.5 Nuclear export – NEP, packaging, budding, and release

The export of vRNPs out of the nucleus require the help of the viral nuclear export protein (NEP), and the interaction between NEP and the vRNP is bridged by M1 [Huang et al. 2012]. Two leucine-rich nuclear export signals (NES1 and 2) on the C-terminal and N-terminal domains of NEP, respectively, are required for recognition and export by the host nuclear export receptor, chromosome region maintenance 1 (Crm1) [Huang et al. 2012]. The vRNPs are shuttled to the cytoplasm via microtubules and arranged for packaging based on specific interactions between vRNA and viral proteins [Fournier et al. 2012]. The vRNPs are incorporated into the progeny viruses at the so-called budozones which form close to lipid rafts populated with viral membrane proteins, HA, NA, and M2 [reviewed in Santos, Chacon & Rosas-Acosta, 2013]. Stabilizing

interactions between M1 and the cytosolic tails of HA and NA are key factors in the budding process [Rossman & Lamb, 2011]. Hydrophobic residues in M1 associate to the membrane side and allow for an interlocking sheet to form [Reviewed in Rossman & Lamb, 2011]. The formation of spherical or filamentous viral particles may be dependent on differences in the membrane curvature induced by M2 [Rossman et al. 2010]. Completion of the budding process does not require the ESCRT complex, as seen with other viruses, but instead, membrane scission is M2 dependent [reviewed in Rossman & Lamb, 2011; Santos, Chacón & Rosas-Acosta, 2013]. Progeny virion are released into the extracellular environment after NA cleaves sialic acids bound to the host cell and from glycoproteins on the viral membrane [Nayak et al. 2009]. Release of infectious particles results in subsequent waves of attachment and replication.

1.4.6 Immune response and NS1

The recognition of pathogen-associated molecular patterns (PAMPs) from infection by influenza activates the innate immune response triggering the release of proinflammatory cytokines and chemokines including interferon (IFN); this is one of the most effective host mechanisms against influenza virus infection [Ehrhardt et al., 2010]. The retinoic acid-inducible gene 1 (RIG-I) is a dsRNA helicase enzyme which recognizes vRNPs, activates the interferon response, and is one target of the viral multifunctional host immune response inhibitor NS1 [Forbes et al., 2013]. The influenza A virus non-structural protein, NS1, interacts with numerous cellular and viral factors due to its ability to translocate between the nucleus and the cytoplasm [Hale et al., 2008]. NS1 is comprised of two domains, the N-terminal RNA binding domain (residues 1-70) and the C-terminal effector domain (residues 86-230) [reviewed in Das et al., 2010]. The N-terminal domain exists in a homodimeric state which binds to dsRNA and is able to block the detection of dsRNA normally facilitated by 2', 5'-oligoadenylate synthetase (OAS) [Min & Krug, 2006]. OAS is IFN induced and activates RNase L which leads to the degradation of cellular and viral RNAs [Randall & Goodbourn, 2008]. By blocking viral RNA detection, NS1 is able to inhibit

both the production of antiviral proteins as well as the host cell apoptotic response [Hale et al., 2008]. NS1 is also reported to inhibit the expression of host genes, including type I IFN, through interactions between its C-terminal domain and the cleavage and polyadenylation specificity factor 30 (CPSF30) in the nucleus, decreasing 3′-end processing of cellular pre-mRNAs [Kochs et al., 2007]. Protein kinase R (PKR), in response to infection, inhibits host translational machinery as a protective measure, this activity is blocked by interactions with the C-terminal domain of NS1 [Min & Krug, 2006].

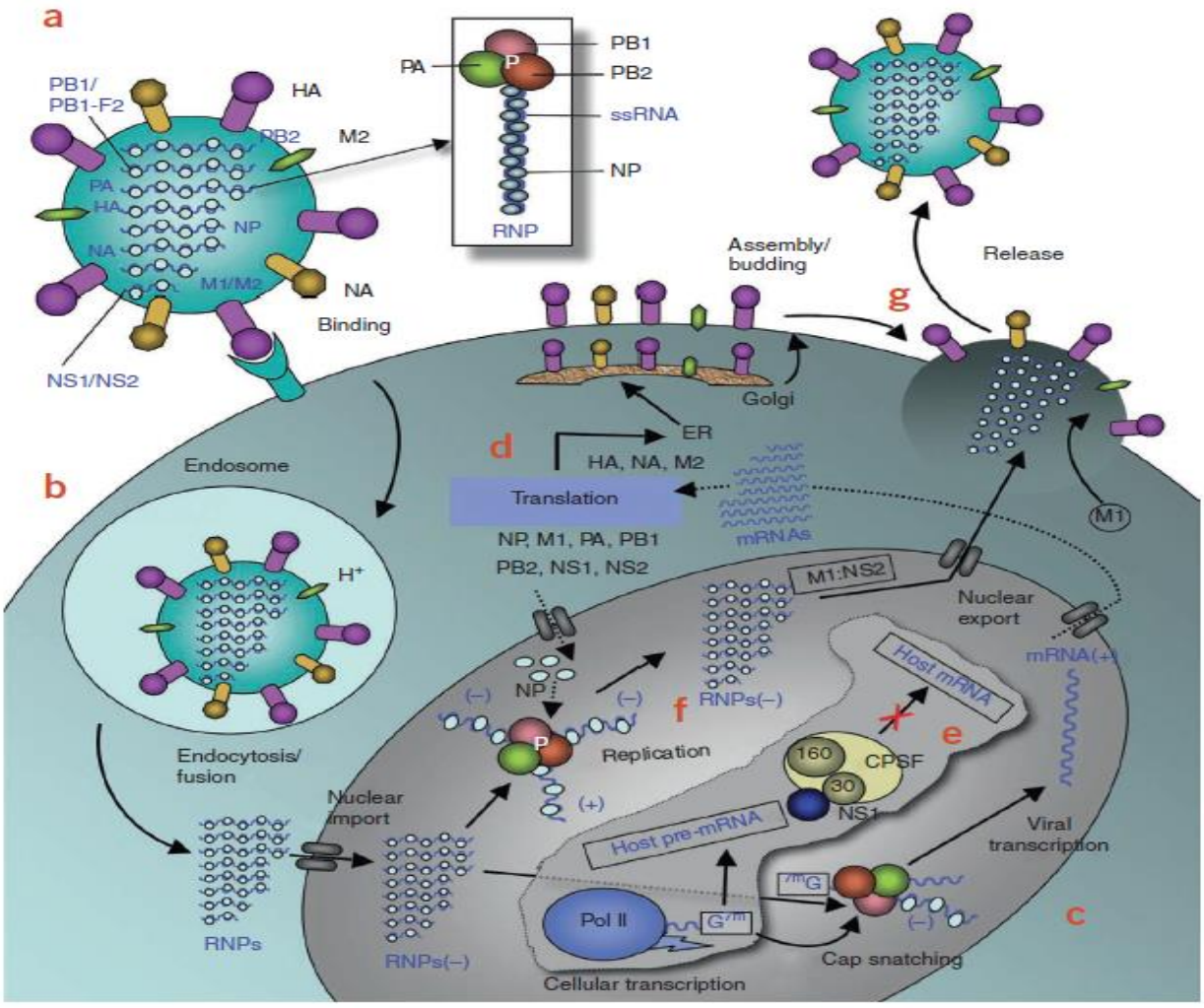

Figure 1.3 Influenza A life cycle.

(a) The viral surface glycoprotein HA binds to the host cell-surface sialic acid receptors (b) entry via endocytosis; acidification results in membrane fusion and dissociation of vRNPs from M1 (c) nuclear import by NLSs is followed by "cap-snatching" for transcription. (d) Early stage proteins are translated for vRNA production and packaging. This is followed by late stage protein synthesis of structural and surface proteins for virion assembly. (e) NS1 blocks mRNA processing and allows for the transport of unprocessed viral mRNA into the cytoplasm. (f) The switch from transcription to unprimed replication produces (-) sense vRNA packaged into vRNPs and shuttled out of the nucleus to the cell membrane through interactions with M1, NEP, and CRM1. (g) vRNPs are incorporated into new viruses that bud out of the cell and require NA cleavage for their final release from the cell surface.

Image from Das, K., Aramini, J. M., Ma, L.-C., Krug, R. M., & Arnold, E. (2010). Structures of influenza A proteins and insights into antiviral drug targets. Nature Structural & Molecular Biology, 17(5), 530–538. http://doi.org/10.1038/nsmb.1779.

1.5 SUMO

1.5.1 SUMO: The Small Ubiquitin-like MOdifier

Ubiquitin-like proteins (Ubls) are a set of post translational modifiers homologous to ubiquitin in structure, including interferon-stimulated gene 15 (ISG15), small ubiquitin-like modifier (SUMO) and NEDD8; however, Ubls are processed, activated, conjugated and deconjugated by a different set of enzymes than those involved in the ubiquitin pathway. [Hochstrasser, 2000; Liu et al., 2013] The Small Ubiquitin-like MOdifier (SUMO) is covalently conjugated to target proteins in a process known as SUMOylation, and results in the modulation of the target protein's stability, activity, localization, and conformation. The downstream affects attributed to this modifier include changes in transcription, DNA repair, and the immune response [Hannoun, Maarifi & Chelbi-Alix, 2016]. SUMO is approximately 11kDa in size but usually runs as a 17kDa protein by SDS-PAGE. SUMO-1,-2,-3, and -4 are the four distinct isoforms found in mammals. SUMO1 shares 50% homology with SUMO2 and 3 which are indistinguishable by antibodies and share 97% identity with each other [Johnson, 2004]. SUMOylation involves three enzymes for conjugation to target proteins. Conjugation occurs through lysine residues and a substantial fraction of known SUMOylation sites are located within the consensus sequence ψKxE, where ψ corresponds to a large hydrophobic amino acid, generally isoleucine, leucine, or valine, K is a lysine residue, x is any amino acid, and E is a glutamic acid residue [Rodriguez, Dargemont & Hay, 2000]. The ψKxE motif is present at the N-terminal region of SUMO2/3 and this allows them to form poly-SUMO chains. SUMO1 lacks this sequence and is therefore considered to act as a SUMO chain terminator [Tatham et al., 2001] (Figure 1.4A).

1.5.2 SUMO basics

SUMO is translated as an immature precursor which requires processing by a SUMO protease. Proteolytic cleavage by SUMO proteases exposes a di-glycine motif that allows for the

now mature form of SUMO to be reversibly conjugated to a target protein [Everett, Boutell & Hale, 2013] (Figure 1.4b). Once in this mature form, SUMO forms an ATP driven thioester linkage between its carboxyl terminus and a cysteine residue in the active site of the E1 activating enzyme; E1 is a heterodimer of SUMO Activating Enzymes SAE1 and SAE2 [Hay, 2005]. SUMO is then transferred directly to the E2 conjugating enzyme, Ubc9, via an analogous thioester bond formation [Hay, 2005]. Ubc9 alone is able to directly recognize and conjugate SUMO to its protein targets through the formation of an isopeptide bond between the di-glycine motif in SUMO and the epsilon amino group of the lysine side chain in the substrate molecule [Wang & Dasso, 2009; Gareau, & Lima, 2010] (Figure 1.4c). The conjugation of SUMO to specific targets can be enhanced by E3 ligase enzymes which act by stabilizing the interactions established between SUMO, Ubc9, and the target protein [Melchior, Schergaut & Pichler, 2003]. The number of proteins characterized as SUMO E3 ligases continues to increase [Kagey, Melhuish & Wotton, 2003], but three main groups of E3 ligases have been characterized to date, namely the protein inhibitor of activated STAT (PIAS) proteins, the Ran binding protein 2 (RanBP2), and the polycomb protein (PC2) [Kagey, Melhuish & Wotton, 2003]. SUMOylation is a transient modification and therefore SUMO is frequently removed from its target shortly after conjugation. The effect of this modification is nevertheless frequently maintained even after deconjugation by proteolytic cleavage. The main family of mammalian SUMO proteases consist of seven sentrin-specific protease (SENP) isoforms which contain C-terminal Ulp domains of varying hydrolase activity [Drag, 2008; Melchior, Schergaut & Pichler, 2003]. Upon being de-conjugated from its target, sumo can be recycled back into the conjugation pathway.

Viruses have evolved numerous mechanisms to hijack host cellular components for optimal replication including the subversion of host defenses. Influenza has been shown to not only interact with the SUMOylation system, but to also require an active SUMOylation system for successful replication, packaging, and optimal protein functionality [Pal et al., 2010; Pal et al., 2011; Mok et al., 2012; Han et al., 2014; Tawaratsumida et al., 2014; Domingues et al., 2015].

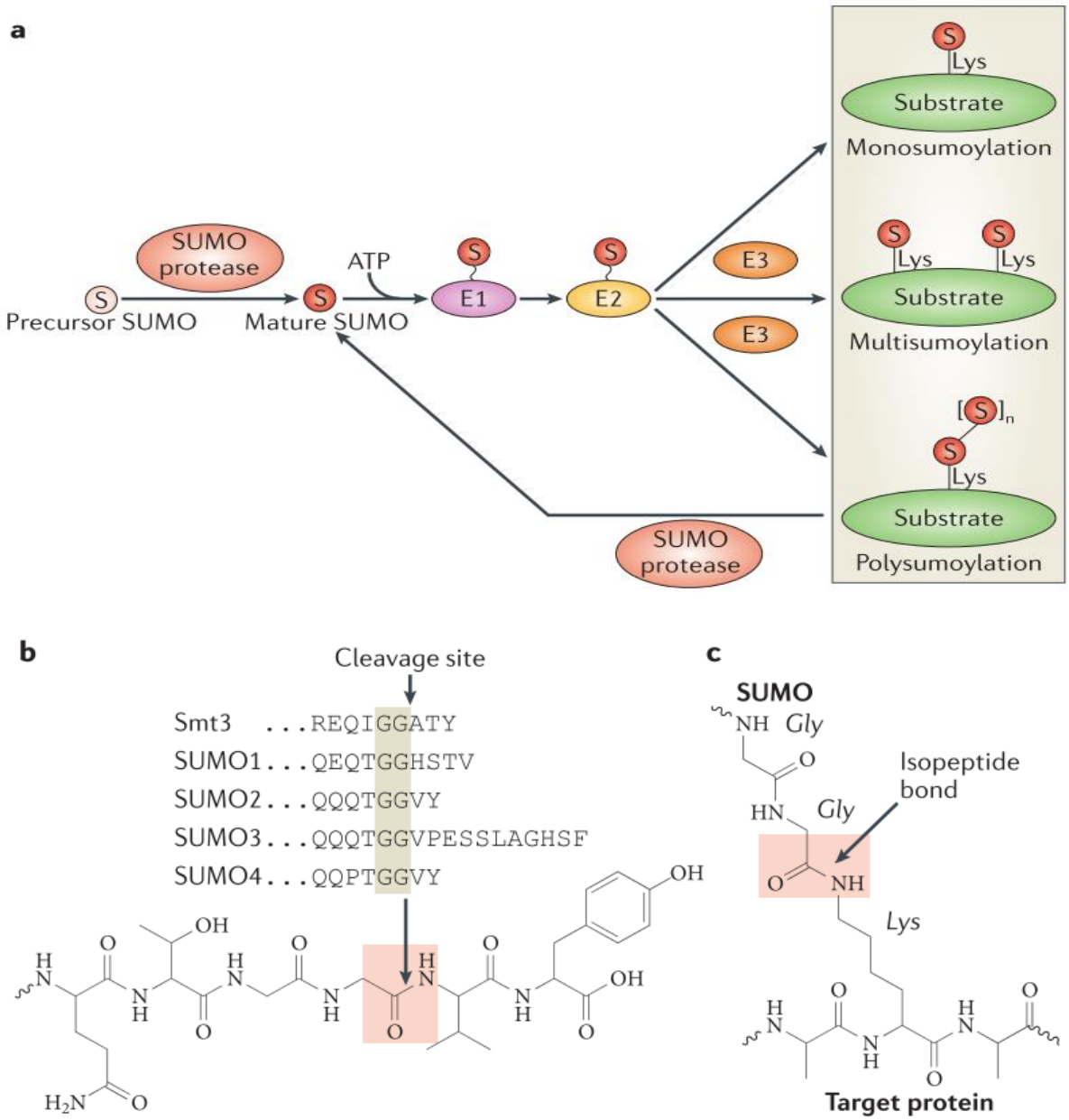

Figure 1.4 SUMOylation Figure.

(a) SUMO activation and enzymatic pathway for conjugation and deconjugation. (b) Proteolytic cleavage at the C-terminal end of SUMO to expose the di-glycine motif. (c) Isopeptide bond formation at the epsilon amino group of the lysine side chain in the substrate molecule.

Image from Hickey, C. M., Wilson, N. R., & Hochstrasser, M. (2012). Function and regulation of SUMO proteases. Nature Reviews. Molecular Cell Biology, 13(12), 755–66. http://doi.org/10.1038/nrm3478.

1.5.3 The cellular SUMOylation system and influenza infection

Protein SUMOylation has been shown to regulate numerous cellular functions. The molecular consequences of SUMO modification are the main focus of current research; however, the factors involved in the signaling and regulation of substrate modification by SUMO are far less characterized and understood. The cellular SUMO profile, both free and conjugated, is known to increase under several known stress inducing conditions including heat shock, hypoxia, and influenza infection [Golebiowski et al. 2009; Hsieh et al. 2013; Santos et al. 2013]. The increase in SUMO2/3 seen during heat shock and hypoxia is reported to be crucial for cellular survival [Golebiowski et al. 2009]. Similarly, increased SUMOylation has been shown to be essential for cell survival under viral infection [Hsieh et al. 2013; Sahin, 2014], even though numerous viral proteins are required to be SUMOylated for optimal function.

Influenza virus interacts with several cellular post-translational modification systems, including glycosylation (which targets HA and NA), palmitoylation (S-acylation of HA and M2), phosphorylation (which regulates NS1 and PB1-F2), ISGylation (which targets NS1), and SUMOylation (known to target M1, NS1, NP, PB1, and NEP reviewed in Matsuoka, Kawaoka et al. 2013; Tang et al. 2010). The non-structural protein NS1 appears to be the most effectively SUMOylated protein during influenza infection [Pal et al. 2011]. Furthermore, the SUMOylation of NS1 at lysine residues 70 and 219 is crucial for its ability to act as an antagonist of the host immune response, and mutations blocking the SUMOylation of these residues results in diminished viral growth [Santos et al. 2013; Xu et al. 2011]. SUMOylation is a mechanism that has proven crucial for both viral propagation and cellular survival. Further research towards understanding the regulatory factors involved with substrate selection and the increase in SUMOylation seen during stress is clearly needed.

1.6 SIGNIFICANCE AND AIMS

Pandemic strains of influenza can easily spread across the globe and with mortality rates likely to reach values as high as 60%, they can pose a serious threat to the human population and global economy. This risk is exacerbated by the proven inability to produce, distribute, and implement an effective vaccine in a timely manner, against a novel pandemic virus. Rather than focusing research resources on the development of vaccines and anti-viral therapies rapidly rendered ineffective by viral mutations, research resources should be expanded to emphasize studies aimed at understanding how influenza is able to interact with and modulate host cellular systems to its advantage. Our research group was the first to show that NS1 is a SUMO substrate and that influenza interacts extensively with the SUMOylation system [PAL ET AL. 2010, 2011]. This was followed by our discovery that NS1 is a key player in the regulation of the SUMOylation system during infection [Santos et al. 2013]. Not only does NS1 require SUMOylation to maintain normal function (immune response antagonist, RNA binding, etc.), but NS1 also needs to be SUMOylated in order to induce a global increase in the SUMOylation profile. This finding, in combination with recent work suggesting that SUMO is heavily involved in the cellular antiviral and stress responses indicate that research in SUMO is clearly needed; identifying regulatory mechanisms of such a vital signaling protein presents valuable discovery potential including immune regulation, cell survival, and cancer related cell maintenance. The use of model regulators of the SUMOylation system will allow for the tracking of specific key interactions. Heat shock and hypoxia are two known environmental stressors capable of triggering increases in cellular SUMOylation. More recently, other labs have reported findings supporting our discovery that influenza infection also causes a Global Increase in Cellular SUMOylation (GICS) and this increase has been suggested to be protective. Remarkably, very little is known about how SUMO is regulated or what role it plays during stress inducing events such as heat shock or influenza infection. **The overarching goal pursued by this project was to standardize the protocols needed to determine whether the global increase in SUMOylation levels that occur during**

cellular stress is the result of transcriptional and post-translational level regulatory mechanisms or a result of other mechanisms governing SUMO conjugation and target specificity of the system.

Specific aims:

The specific goals of this project will focus on the optimization of protocols for all key techniques needed to consistently quantify transcripts from cells as well as to efficiently conduct immunoprecipitations in future proteomic studies. The experiments that will be able to be performed following this optimization will address potential regulatory mechanisms involved in dictating cellular SUMOylation levels.

Aim 1:

To develop techniques needed to consistently quantify transcript levels with high accuracy, several protocols require standardization. These techniques will be used by future researchers to measure changes in steady state transcript levels of any gene using GAPDH as a positive control and loading control. For this optimization, transcript levels of SUMO1 and GAPDH will be measured after the induction of the Global Increase in Cellular SUMOylation (GICS) under the constraints of three known factors. GICS induction was standardized using heat shock, hypoxia, and influenza infection; all of which are reported to cause a marked increase in the SUMOylation profile. Previous studies have attributed the cellular stress response to almost exclusively involve SUMO2/3, but present studies by our lab and others have shown the SUMO1 profile to also fluctuate significantly after exposure to specific stress factors, including heat shock, hypoxia, and influenza infection [Rosas-Acosta et. al. 2005]. After treatment, purification of total RNA using a commercially available kit will be optimized. RNA quantification, by RNA gel electrophoresis followed by cDNA synthesis is required to create a template that can be used for quantitative PCR. To set up and analyze cDNA by qPCR, using SYBR Green as the reporter, will require two levels

of optimization; *i)* preparation of all components involved in the reaction and *ii)* optimization of the settings required to perform quantitative PCR and analysis. cDNA synthesis (two long temperature stages – resulting in single stranded cDNA equal in copy number to starting mRNA) is followed by real time qPCR using sequence specific primers in combination with SYBR Green intercalating reference dye. Measuring transcript levels before and after triggering GICS as well as the change in SUMO1's mRNA profile after IAV infection, with a strain that codes for a non-SUMOylatable version of NS1, will provide insight towards the possibility that regulation may or may not occur at the transcriptional level. The NS1

SUMOylation deficient mutant does not cause a GICS and has a significant reduction in growth by plaque assay, but it is highly virulent in a mouse model. Currently, published and unpublished data suggests that NS1 needs a narrow range of SUMOylation for proper dimerization, RNA interaction, and other protein-protein interactions. Interestingly, the increase in virulence seen in the non-SUMOylatable mutant continues to support the hypothesis that SUMOylation is a protective response and influenza has the ability to modulate the system for maximum cell viability and optimal viral replication.

Aim 2:

To further characterize SUMO target selection during stress, all SUMO modified proteins will be identified. The second aim of this project was designed to optimize the protocols needed to identify the SUMO1 target profile before and after the induction of GICS. This study will also account for the differences seen in both strains of IAV – wild type (WT) and the virus containing a non-SUMOylatable NS1 – Double Mutant (DM). Using these two models to highlight the differences in SUMO1 targeting may bring to light crucial interactions needed for optimal cell viability after infection. The SUMO1/substrate samples immunoprecipitated from a tissue culture model will be analyzed by mass spectrometry. To collect a sufficient amount of protein required for analysis, a large amount of antibodies against SUMO1 were needed. We have recently obtained

hybridoma cells that produce a very specific and sensitive monoclonal anti-SUMO1 antibody. These cells were used to synthesize milligrams of anti-SUMO1 antibody. Optimization of this entire process is needed to efficiently produce antibodies in large amounts. The hybridoma cells will be grown in tissue culture and tested before inoculating a balb/c mouse via Intraperitoneal injection (IP). The subsequent ascites that develops in the abdominal cavity of the mouse will contain a large volume of relatively pure IgG at high concentrations. The antibodies were immobilized on protein G beads, incubated with the lysate of treated cells, collected using a column, and the bound proteins captured by the anti-SUMO1 antibodies were eluted. The differentially SUMOylated set of proteins will be categorized by function and may be further investigated as key regulators in future research.

Altogether, this project provides a detailed account of the standardization of protocols needed to study the changes in SUMOylation. The three models that will be used to consistently induce increases in SUMOylation (cause GICS) include: heat shock, hypoxia, and influenza infection. These protocols were standardized and verified by immunoblot for future use in this lab. After the induction of GICS using each model, future experiments will measure changes in steady state levels of mRNA and changes in substrate targeting. These findings will assist in the identification of potential regulatory processes involved in the SUMOylation pathway. SUMO has been shown to rival ubiquitin in function and an increasing number of research groups continue to find the post translational modifier to be closely tied to cellular stress and antiviral responses. This finding alone warrants an increase in research focused towards understanding the regulation of this protein which could potentially be the key to understanding the stress response on a cellular level.

Chapter 2: Quantifying SUMO transcript expression by quantitative Reverse Transcription - Polymerase Chain Reaction (qRT-PCR)

2.1 INTRODUCTION

An increase in the SUMO1 profile, both free and conjugated, is observed after exposure to several known factors. These factors are also known stress response triggers; they induce GICS similarly but with distinct differences. Due to their ability to induce GICS similarly, these three independent types of stress (heat shock, hypoxia, and infection by several viruses including influenza) can serve as models to be used for the investigation of potential regulatory mechanisms involved in the SUMOylation pathway. The goal of this aim is to determine if the inducible increase in SUMOylation is achieved by the modulation of one specific gene, SUMO. Previous studies by Rosas-Acosta et al. 2004, Pal et al. 2010, and Hale 2015, have determined that the increased SUMOylation is not caused by the increased synthesis of SAE2,1 or Ubc9 (the conjugating enzymes required for SUMOylation). Rather, the increase may be a result of a number of other factors including; increased Ubc9 activity, alternative splicing of the SUMO1 transcript rendering some forms more active, an increase in SUMO stability, microRNA regulation, or a decrease in de-SUMOylation. Another alternative may involve an increase in the translation of SUMO1 transcripts, typically associated to increases in the polysomal fraction – multiple ribosomes actively translating mRNA coding for SUMO1. The regulation of SUMO1 may still be a result of altered substrate targeting which will be the focus of my second aim.

Upon viral infection, the non-structural protein (NS1) encoded by the eighth gene segment of influenza A begins its journey in the subversion of the host cell. A major function attributed to NS1 is its ability to inhibit the host immune response. As a result, the virus is able to evade the cytoplasmic checkpoint of dsRNA recognition mediated by RIG-I (Hale et al. 2008). In a similar manner, NS1 is also able to inhibit the antiviral responses regulated by the PKR (recognition of

dsRNA) and OAS (triggers RNA degradation during viral infection) proteins [Kochs et al. 2007]. NS1 ultimately prevents the activation of Interferon Regulatory Factors (IRFs) as well as other antiviral factors, however, the majority of NS1's known functions appear to be dependent on modification by SUMO1 [Pal et al. 2009; Santos et al. 2013]. The article published by, Santos et al. 2013, demonstrates that SUMOylation of NS1 modulates its ability to form dimers and in turn, its ability to bind to RNA [Hale, 2008; Engel, 2013]. It is vital to take note that only upon SUMOylation, does NS1 acquire the ability to induce a Global Increase in Cellular SUMOylation termed GICS [unpublished data]. Cell lines infected by a strain of influenza containing a non-SUMOylatable form of NS1 (double mutant - DM), developed by our lab, show a decrease in viral propagation and a loss in the ability to trigger the GICS normally associated with infection. This same SUMOylation deficient virus exhibits a distinct difference in growth and pathogenicity when studied in a mouse model. It does not induce GICS but does result in increased viral pathogenicity and mortality [unpublished data]. Comparing the changes in the SUMOylation profile after infection with viruses containing either the WT or DM form of NS1 will allow us to determine whether increased SUMOylation is accompanied by changes in SUMO transcript abundance. NS1 may interact with factors involved with the activation of SUMO1 transcription. Changes in SUMO1 mRNA levels after infection, heat shock, or hypoxia would suggest that there are factors imposing one or more regulatory mechanisms at the transcriptional level of processing. The goal of this aim is to identify if the Global Increase in Cellular SUMOylation seen by protein analysis is a result of increased levels of SUMO1 mRNA.

2.2 MATERIALS AND METHODS

Cells and viruses

HEK293FT cells (Invitrogen Corp., Carlsbad, CA), **MDCK cells** (ATCC, Manassas, VA) and **A549 cells** (ATCC) were maintained in complete medium consisting of 1x Dulbecco's modified eagle medium (DMEM) supplemented with high glucose, L- glutamine, sodium pyruvate

(Corning Incorporated Life Sciences, Corning, NY), and 10% fetal bovine serum (Atlanta Biologicals, Inc., Flowery Branch, GA). For HEK293FT cells, Geneticin (Invitrogen Corp.) was added to the complete medium at a final concentration of 500μg/mL. All cell lines were maintained at 37°C and at 5% CO2.

Influenza A/Puerto Rico/8/1934 H1N1 (referred to as PR8) was a gift from John M. Quarles (Department of Microbial and Molecular Pathogenesis, College of Medicine, Texas A&M Health Sciences Center). PR8, and all other viruses, were propagated in MDCK cells at a multiplicity of infection (MOI) of 0.001 by using 1x DMEM supplemented with 0.2% bovine serum albumin (BSA) and 2 μg/mL tosyl-phenylalanyl-chloromethyl-ketone (TPCK)-treated trypsin (Worthington Biochemical Corp., Lakewood, NJ). The virus was titered as described below.

A/WSN/1933 (referred to as WSN) and the non-SUMOylatable NS1 strain WNS/T7T7[NS1K70AK219A~NS2] (Double Mutant) used in this study were generated as previously described [Santos et al. 2013]. Briefly, the A/WSN/1933 [H1N1] 12-plasmid reverse genetics system [Neumann et al. 2000] was provided by Yoshihiro Kawaoka (Department of Pathobiological Sciences, School of Veterinary Medicine, University of Wisconsin-Madison, Madison, WI). WSN viruses were propagated and titered as described for all viruses. Two strains were created previously from the 12-plasmid reverse genetics system and used in this experiment. NEP, as a splicing variant of the NS gene segment, was shifted to eliminate errors induced by mutations made to NS1. The NEP or NS2-shifted constructs used are WSN/T7T7[NS1~NS2] (WT) and WSN/ T7T7[NS1K70AK219A~NS2] (DM). The addition of T7 tags and the shifting of NEP did not result in significant differences in viral propagation [Santos et al. 2013]. Cells infected at an MOI of 10 are removed from the plate after 18 hours and treated with RNeasy lysis buffer (following manufacturer's suggestions) for RNA extraction or 4x Sample Buffer + 10% β Mercaptoethanol for analysis by SDS-PAGE and immunoblot.

Plasmids

pcDNA5/FRT/TO is a vector used for transfection and alone does not encode for proteins.

pcDNA5/FRT/TO/His-SUMO1/IRES/His-Ubc9 is a dual expression construct, used for transfection, that not only causes an increase in the SUMO and Ubc9 proteins, but also causes an increase in SUMOylation of a wide range of proteins; this construct was previously developed and described [Pal, et al. 2009; Santos et a. 2013].

pCMV6-XL5/GAPDH is a construct that after transfection will induce an increase in the total pool of GAPDH and will be used to validate the qRT-PCR results.

pcDNA3/Pol2/T7T7NS1-PR8 #2 codes for a double T7 tagged NS1 protein from the PR8 strain.

pcDNA3/Pol2/T7T7[NS1~NS2] was used to create and generate the recombinant virus WSN/T7T7[NS1~NS2].

pcDNA3/Pol2/T7T7/NS1K70AK219A~NS2 used to generate the recombinant virus WNS/T7T7[NS1K70AK219A~NS2].

Primers

PolyT_cDNAsynth.RV (5' - TTT TTT TTT TTT TTT TTT - 3') was ordered from **Integrated DNA Technologies (IDT - Coralville, IA)** and will be used to uniformly create single stranded cDNA from the pool of total RNA purified from cell culture by reverse transcription.

The following gene-specific primers were used in previous studies to measure SUMO1, and GAPDH (Moore et al. 2013; Schmittgen & Zakrajsek, 2000) and will be used to quantify transcript levels using **StepOnePlus Real-Time PCR System (ThermoScientific)** and associated software.

SUMO1_qPCR.FW (5' – GGA GGC CAA ACC TTC AAC TGA GG – 3')

SUMO1_qPCR.RV (5’ – CCC CGT TTG TTC CTG ATA AAC TTC AAT CAC – 3’)

GAPDH_qPCR.FW (5' – GAT CCC TCC AAA ATC AAG TGG G – 3')

GAPDH_qPCR.RV (5' – GCA GGT TTT TCT AGA CGG CAG G – 3’)

RT-qPCR equipment

For **DyNAmo Flash SYBR Green (ThermoFisher #F415S)** detection, real time PCR primer products should be between 50-200 base pairs and should target a central region of the transcript to avoid quantification errors caused by degradation of the 5' and 3' ends.

Transient transfections

HEK293FT cells (Invitrogen Corp.) were seeded at a density of 3 x 10^5 cells/well into 6 well plates. 24 hours later, cells were transfected by liposome-mediated transfection using 5 µg of CsCl-purified plasmids and 15 µL of TransIT-LT1 (Mirus Bio LLC, Madison, WI) per well, according to the manufacturer's recommendations. Cells were incubated at 37ºC, 5% CO2, for 36 hours. This incubation period was followed by both the collection of cells for RNA extraction and analysis by SDS-PAGE and immunoblot.

TCID50 to determine viral titers

MDCK cells were plated into 96-well plates at a density of 1.6 x 10^5 cells/well in 1x DMEM supplemented with 10% FBS and incubated at 37°C in 5% CO_2 until the cells formed a confluent monolayer. The cells were then washed once with 1x DMEM, and a virus dilution prepared in 1ml of 1x DMEM supplemented with 0.2% BSA was added to the cells and incubated with the cells at 37°C in 5% CO_2 for a minimum of 3 days or until cytopathic effects (CPE) were observed, upto a maximum of 7 days post-infection.

Hemagglutination Assay

50µL of supernantant from TCID50 plates were transferred to a 96-well V-bottom plate (Corning Incorporated Life Sciences). 50µL of 0.5% turkey red blood cells (Lampire Biological Laboratories, Pipersville, PA) suspended in 1x PBS, were added to the V-bottom plate and gently

tapped to mix. Plates were incubated at room temperature for 45 minutes. Plates were scored and viral titers were determined using the Reed-Muench method.

Heat Shock

1mL of otherwise untreated A549 cells adjusted to $8x10^6$ cells/mL was placed in a microfuge tube and held at 45ºC in a water-bath for 45 minutes. The tubes were then centrifuged at 6,000 RPM for 30 seconds to pellet the cells. The supernatant was removed and the pellet was treated with RNeasy lysis buffer for RNA extraction or 4x Sample Buffer + 10% β Mercaptoethanol for analysis by SDS-PAGE and immunoblot.

Hypoxia

Cells were treated with 125μM $CoCl_2$ (Cobalt (II) Chloride hexahydrate) for 24 hours at 37°C in 5% CO_2 to induce hypoxic like conditions. The supernatant was removed and the cells were treated with RNeasy lysis buffer for RNA extraction or 4x Sample Buffer + 10% β Mercaptoethanol for analysis by SDS-PAGE and immunoblot. Induction of hypoxia will be verified by the presence of HIF-1alpha protein at approximately 115kDa by immunoblot.

RNA purification and cDNA first strand synthesis

Total RNA was extracted using both the **QiaShredder** and **RNeasy Mini Kits (Qiagen).** RNA was quantified by agarose gel electrophoresis and fluorescence densitometry of 28s rRNA as a reference, and subsequently used for cDNA synthesis using the **M-MLV Reverse Transcriptase (Promega, Madison, WI)** and **PolyT_cDNAsynth.RV primer** to target the polyadenylated 3' ends of all mRNA following kit recommendations (detailed below).

Total RNA extracted from cell extracts was prepared for quantification by adding 3/4x loading buffer containing formamide to preserve the RNA from degradation and formaldehyde to denature the RNA for gel electrophoresis. The samples were loaded into a 1% agarose gel

containing MOPS buffer, formaldehyde, and ethidium bromide for detection, ran for 70 minutes at 100 volts. The 18s and 28s rRNA will be visible at 1,900bp and 5,000bp, respectively. The cDNA product and primers were tested for functionality by PCR before continuing to qPCR with SYBR Green. The same gene-specific primers were used in combination with SYBR Green to calculate the absolute copy number by qPCR.

Qiashredder (purple tube)

a. Add 350µL of RTL Buffer (cell lysis) to $1x10^7$ cells total
b. Mix well to assist with lysis add to purple Qiashredder tube
c. Spin 30sec 12,000 rpm
d. SAVE FLOW THROUGH
e. Add 350µL 70% EtOH (make fresh) to the FT
f. MIX WELL – this is very important
g. Transfer total volume (700µL) to the pink RNeasy tube

RNeasy

a. Spin down the 700µL - 12K 30sec
b. Discard FT
c. Wash cartridge – 100µL RW1 Buffer then spin - 12K 30sec
d. Wash cartridge 2x – 500uL RPE – 12K 30sec
e. Repeat D

Elution

a. Add 30uL of super clean QH2O (for qPCR)
b. Wait 1 min
c. Spin 12K rpm 30sec
d. Re-use 30uL to re-elute
e. Wait 1 min
f. Spin 12K rpm 30sec
g. Aliquote 5uL per tube – Freeze at -80^0C

Quantification by Electrophoresis

a. 4µL for gel and 1uL for nanodrop
b. RNA quantification
    i. To the 4µL of RNA add

ii. 12µL ¾x Loading Buffer
- 62.88% Formamide
- 6.9% 20x MOPS
- 22.7% Formaldehyde
- 6.9% Glycerol
- 50µL 2% Bromophenol Blue

iii. Heat 65^0C 5min – Chill on ice

iv. Run on Formaldehyde gel (cast and run under the chemical hood) 100v for 70min
- Agarose……..1.8g
- 20x MOPS……..9mL
- QH2O…….....166.5mL
- Boil then add
- Ethidium Bromide [10 mg/ml]……1.8µL
- 10% Formaldahyde……9.7mL

v. 20x MOPS
- 42g MOPS
- 6.8g sodium acetate (mw 136.08)
- 20 mL 0.5 M EDTA
- 400 mL H2O
- pH to 7.0
- bring up to 500mL

cDNA Synthesis Prep [1µM = 1pMol/µL]

a. RATIO - Use 2µg of RNA : 2.5µL 18T.RV Primer [10mM]
b. 1µL RNA 2µg/µL + 2.5µL 18T.RV primer
c. Bring up to 15µL with QH2O
d. Heat 70^0C for 5 min
e. Ice to stop annealing
f. Make a second tube for No Reverse Transcriptase (NRT) – IMPORTANT

cDNA Synthesis PCR

a. Add 5µL of M-MLV (Cat# M1701 Promega, Madison, WI)
b. M-MLV Mix 1x
   vi. QH2O……..13.375µL
   vii. M-MLV Buffer……5.0µL
   viii. 10mM dNTPs……..5.0µL
   ix. RNasin……0.625µL
   x. M-MLV RT……..1.0µL (with ROX already mixed in)
c. Cycle Conditions

xi. 42^0C – 1 hour
xii. 70^0C – 10 min
xiii. 4^0C – hold

d. Store at -80^0C

qRT-PCR

Transcript copies are identified as the cDNA is replicated by PCR using gene specific primers to create <200bp double stranded DNA segments that allow for the intercalation of SYBR Green fluorescent dye. The subsequent quantification is accomplished through the use of plasmids of known copy number and the comparison is based off of the number of cycles needed to reach the Ct (threshold cycle).

SYBR Green Mix **(ThermoFisher #F415S)** requires a passive ROX reference dye dependent on the qPCR machine (included in the kit - do this when it arrives the first time to avoid error in measurement). Half of the total volume experimental sample is SYBR Green. StepOne™ Real-Time PCR Systems includes software to plan the experiment including volumes and controls.

Cycle Conditions

SUMO1

1. 95^0C……10 min
2. 95^0C……30 sec
3. 58.5^0C……30 sec
4. 68^0C……30 sec
5. Go To 2……31x
6. 68^0C……10 min
7. 4^0C……hold

GAPDH

3. 56^0C……....30 sec

Immunoblot analysis

Prior to SDS-PAGE analyses, all cell extracts generated were passed several times through a 29½-gauge needle to break down genomic DNA and decrease viscosity. β-mercaptoethanol was added up to a final concentration of 10%, and the samples were boiled in a bead bath for 10 minutes. The samples were resolved using SDS-PAGE gels made in-house and, subsequently, the proteins were transferred to Immobilon-FL (Millipore Corp., Bedford, MA) for use with IRDye-conjugated secondary antibodies (LI-COR Biosciences Inc., Lincoln, NE) and infrared fluorescence imaging.

Infrared fluorescence imaging

Immobilon-FL membranes (Millipore Corp.) were washed four times in 1x PBS, blocked with Odyssey Blocking Buffer (LI-COR Biosciences Inc.) for a minimum of 1 hour at room temperature, and incubated in Odyssey Blocking Buffer plus 0.1% polysorbate 20 (Tween 20) at 4°C overnight with the primary antibody at the indicated dilution (**anti-SUMO1 Y299 Abcam, 1:2000; anti-GAPDH AB2302 Millipore, 1:2000; anti-β Actin ab8227 Abcam, 1:5000; and anti-M1 ab20910 Abcam, 1:2000; anti-HIF-1-alpha ab51608 Abcam, 1:1000**). The membranes were then washed four times with 1x PBS, supplemented with 0.1% polysorbate 20 (Tween 20), and incubated with secondary antibodies diluted in Odyssey Blocking Buffer plus 0.1% polysorbate 20 (Tween 20) for 1 hour (**IRDye 800 CW- and IRDye 680 LT-conjugated secondary antibodies LI-COR Biosciences Inc. 1:20,000**). The membranes were then washed two times with 1x PBS, supplemented with 0.1% Tween 20, three times with 1x PBS and scanned on an Odyssey CLx infrared imaging system (LI-COR Biosciences Inc.). Quantitative analyses of the images obtained was performed by using Odyssey Infrared Imaging System Application software version 3.0.29 (LI-COR Biosciences Inc.). Statistical analyses and graphics of the data generated were performed by using GraphPad Prism version 5.04 for Windows (GraphPad Software Inc., San Diego, CA).

Statistical analysis and computer software.

All statistical analyses and graphics presented were performed by using GraphPad Prism version 5.04 for Windows (GraphPad Software Inc.). All figures were created by using Adobe Photoshop CS5 extended version 12.0.3 X64 (Adobe Systems Inc., San Jose, CA).

2.3 RESULTS

Inducing Global Increases in Cellular SUMOylation using several proven models. Future studies aimed at measuring changes in steady state transcript levels from Eukaryotic cells must satisfy several procedural steps, verified by quality control, for optimal efficiency: *i)* treatment, *ii)* collection of RNA, *iii)* quantification of RNA*, iv)* primer validation*, v)* qPCR pretest, *vi)* Final qPCR. For this project, three treatments will be used to induce an increase in SUMOylation. Standardization of the models being used as GICS induction factors is the initial step required for reproducibility.

Heat Shock:

Increasing the temperature of cells until 'heat shock' is achieved requires the several factors to be accounted for. Heat shock has to occur across all cells rapidly and for a set amount of time. Protocols previously used to induce heat shock for monitoring changes in the SUMO profile recommend the incubation of cells at 42^0C for 30 minutes [Golebiowski, 2009]. This was improved by the removal of the cells from the culture plate and the use of a water bath to maximize time spent at heat shock inducing temperatures. The optimal settings for heating cells to adequately induce increases in SUMOylation were 45 minutes at 42^0C (Fig. 2.1). Substantial increases in SUMOylation can be seen at the 42kD, 50kD, and high molecular weight ranges by immunoblot.

Hypoxia:

To deprive cells of oxygen below normal levels requires either the use of a hypoxic chamber, a cell culture incubator with nitrogen, or through the addition of a chemical inducer of hypoxia, such as Cobalt Chloride (Cobalt (II) Chloride hexahydrate) - $CoCl_2$, for 24 hours [Hsieh et al. 2013]. Concentrations from 1mM to 31.3μM were tested and compared to the positive control for GICS - influenza infection (Fig. 2.2). A distinct change in the SUMO1 profile was seen between basal SUMO levels and the most effective concentration of 125μM seen at the 25kDa and 65kDa ranges. This increase in SUMOylation was also seen in the positive control of IAV infection. Cobalt Chloride was used to mimic hypoxia but the indicator protein, HIF-1α, was not visible as the antibodies used were defective. This method was functional and may be simple to implement, however, it may not be a completely reliable, reproducible, or as effective as using a hypoxic chamber. $CoCl_2$ may not accurately mimic hypoxic conditions because it becomes less effective over time as it continuously scavenges oxygen from the environment and because cobalt chloride can be disproportionately distributed between wells.

Influenza infection:

An increase in cellular SUMOylation had been observed upon the infection of a variety of cell lines. Transfection of A549 cells with the gene segment that codes for NS1, pcDNA3/Pol2/T7T7[NS1~NS2], causes an increase cellular SUMOylation (Fig. 2.3). Influenza infection as well as the transfection of NS1 both cause GICS as characterized by the appearance of newly SUMOylated bands at 40, 52, and a third band between 70 and 90kDa. The NS1 protein from the WSN strain has a dramatic increase over PR8 (pcDNA3/Pol2/T7T7NS1-PR8 #2), as well as when compared to its mutated non-SUMOylatable form (pcDNA3/Pol2/T7T7/ NS1K70AK219A~NS2) (Fig 2.3). Due to its ability to induce GICS at higher levels, the recombinant virus containing this same NS1 was used to infect A549 cells at an MOI of 10 for 24 hours (Fig 2.4). The appearance of newly SUMOylated bands at the 40, 52, and 90kDa ranges

provide verification that this virus is capable of inducing GICS. The time frame needed to best visualize infection-mediated increases of SUMOylation has not previously been standardized. The aim of this section was to identify the hours post infection that result in optimal increases in SUMO visible by immunoblot. This was achieved by a completing a time course experiment to standardize the duration of infection (Fig. 2.5). Infection inducing the most prominent increases in SUMOylation occurred after the 16-hour time point. Infection lasting 24 hours resulted in a slight decrease in total SUMO signal and will not be used for future GICS related experiments.

RNA extraction and quantification:

After all treatments are completed, collection of RNA is a crucial step to avoid a loss in quality due to cross contamination, a loss in accuracy due to inaccurate measurement, and a loss in yield as a result of degradation. Optimal settings used for the final elution step of the RNeasy kit were tested (Fig. 2.6). Using 70% ethanol made ahead of time resulted in decreased yield (lane 1). Extracting RNA from two times as many cells than the kit suggests (lane 2) resulted in yields similar to lane 4. The third variation was to perform a second elution of one sample using the same 30µL of QH_2O and this resulted in an extreme increase in total yield (lane 4). However, a second elution of one sample using a fresh 30µL of QH_2O (for a final volume of 60µL) resulted in a diminished concentration of RNA; taking into account the increase in total volume (lane 3). After the collection of RNA using the RNeasy kit, total RNA must be quantified. Prepared samples were resolved using formaldehyde agarose gel electrophoresis and UV followed by densitometry. RNA concentration was then adjusted to uniform levels and further optimized for cDNA first strand synthesis. This step was followed by cDNA synthesis and storage at -80^0C.

Primer check:

Primers were designed as previously described by Moore et al. and Schmittgen et al. Optimal annealing temperature for each set of primers was determined by using a gradient of

temperatures around the indicated melting temperature (Fig. 2.7). SUMO1 primers worked most efficiently at 58.5^0C with a product at 250 base pairs (Fig. 2.7 left) The GAPDH primer produced the highest amount of 500bp product at 56^0C (Fig. 2.7 right).

RT-qPCR optimization:

Before the full quantification of steady state mRNA is performed, a final validation experiment was conducted. This final optimization experiment tested the cDNA synthesized after RNA quantification, the negative control – NTC, the SYBR Green polymerase, and the plasmid dilutions standards used for absolute quantification (Fig. 2.8). The reaction was performed using a thermo-cycler PCR machine for 30 cycles with the optimized annealing temperatures. The negative control containing no DNA (NTC) returned no product when incubated with either primer set. The cDNA was functional and at an adequate concentration as the product was present for SUMO1 and GAPDH at 250bp and 500bp, respectively. The five dilutions of each plasmid produced double stranded DNA fragments of the expected size. All of the components needed for accurate quantification of SUMO1 and GAPDH transcripts including SYBR Green were functional.

Positive control validation:

To validate our ability to quantify changes in transcript levels by RT-qPCR, cells were transfected with one of three plasmids. A non-coding plasmid (#23), a dual expression construct, used in previous research by Santos et al. 2013, that induces increases in free and conjugated SUMO1 (#28), and a plasmid coding for GAPDH (#453). The cells were collected 36 hours post transfection. The purified RNA was quantified and used for cDNA synthesis. The Step-One qPCR machine and software was used with SYBR Green to quantify steady state transcript levels (Table 2.1). Both the SUMO1 (Table 2.1A) and GAPDH (Table 2.1B) transfected cells showed to have a dramatic increase in transcripts (Fig. 2.9). Increased transcript levels result in a decrease in Ct

values. The Tm value is used to verify that the product being measured is indeed the same in all samples.

Influenza infection and heat shock:

Steady state mRNA levels of SUMO1 were measured from cells infected with WNS/T7T7[NS1~NS2] at an MOI of 10 for 18 hours and cells that underwent heat shock at 42^0C for 45 minutes (Fig 2.10). SUMO1 values were normalized to GAPDH and did not have statistically significant changes in quantity after heat shock or infection. The influenza infected cells did show a small decrease in SUMO1 transcript levels as seen by an increase in the number of cycles needed to reach Ct (Fig 2.10A). The absolute copy number was calculated to have a similar change (Fig 2.10B).

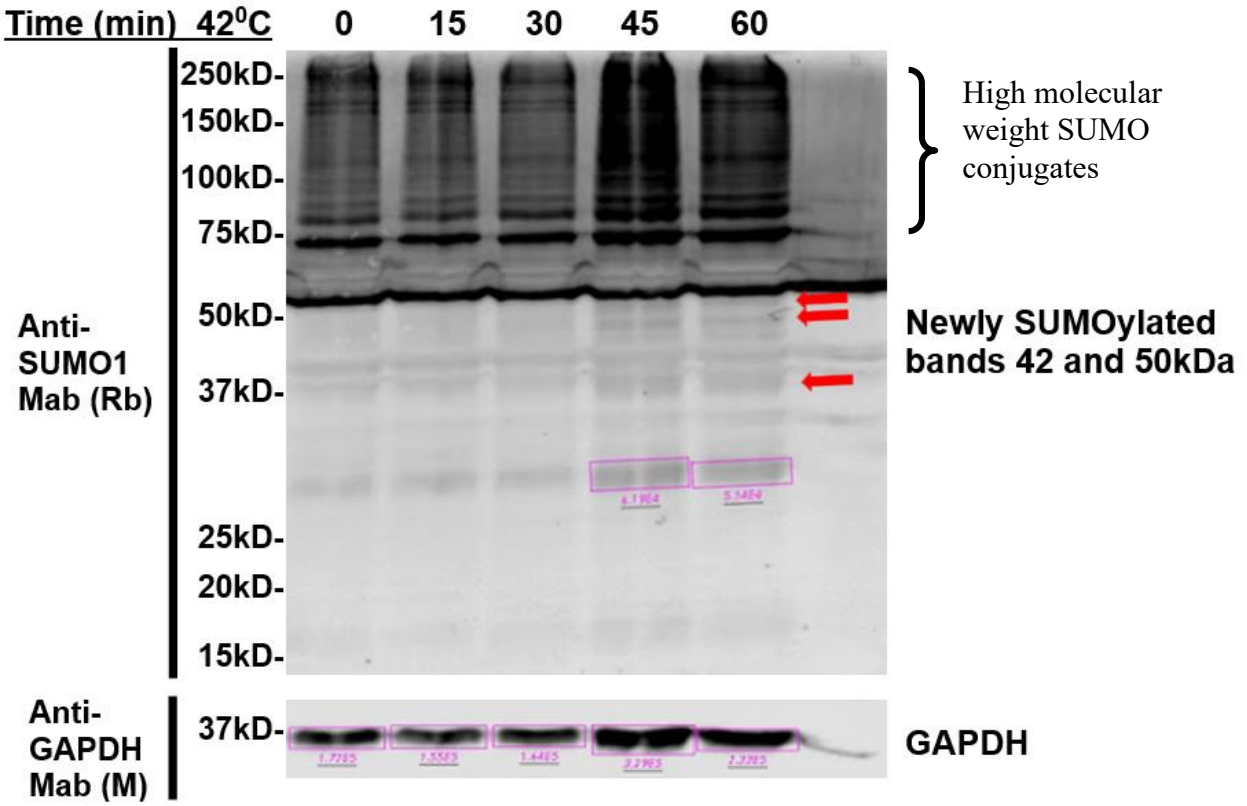

Figure 2.1 Inducing GICS of SUMO1 with the heat shock model.

A549 cells were re-suspended in sterile 1xPBS, transferred to a microfuge tube, and held at 42oC in a water-bath for 45 minutes. The cells were collected and treated for analysis by SDS-PAGE and immunoblot. Samples collected prior and up to 30 minutes into the heat shock process did not result in any visible changes in the SUMO1 profile. The increase in the SUMO1 profile, seen at 42 and 50kDa, occurs at 45 minutes and slightly diminishes at the 60-minute time point. A substantial increase in SUMOylation, between 75 and 250kDa, is also seen after 45 minutes of heat shock. Monoclonal antibodies (Mab) from rabbit (Rb) and mouse (M) were used to identify SUMO1 and GAPDH, respectively.

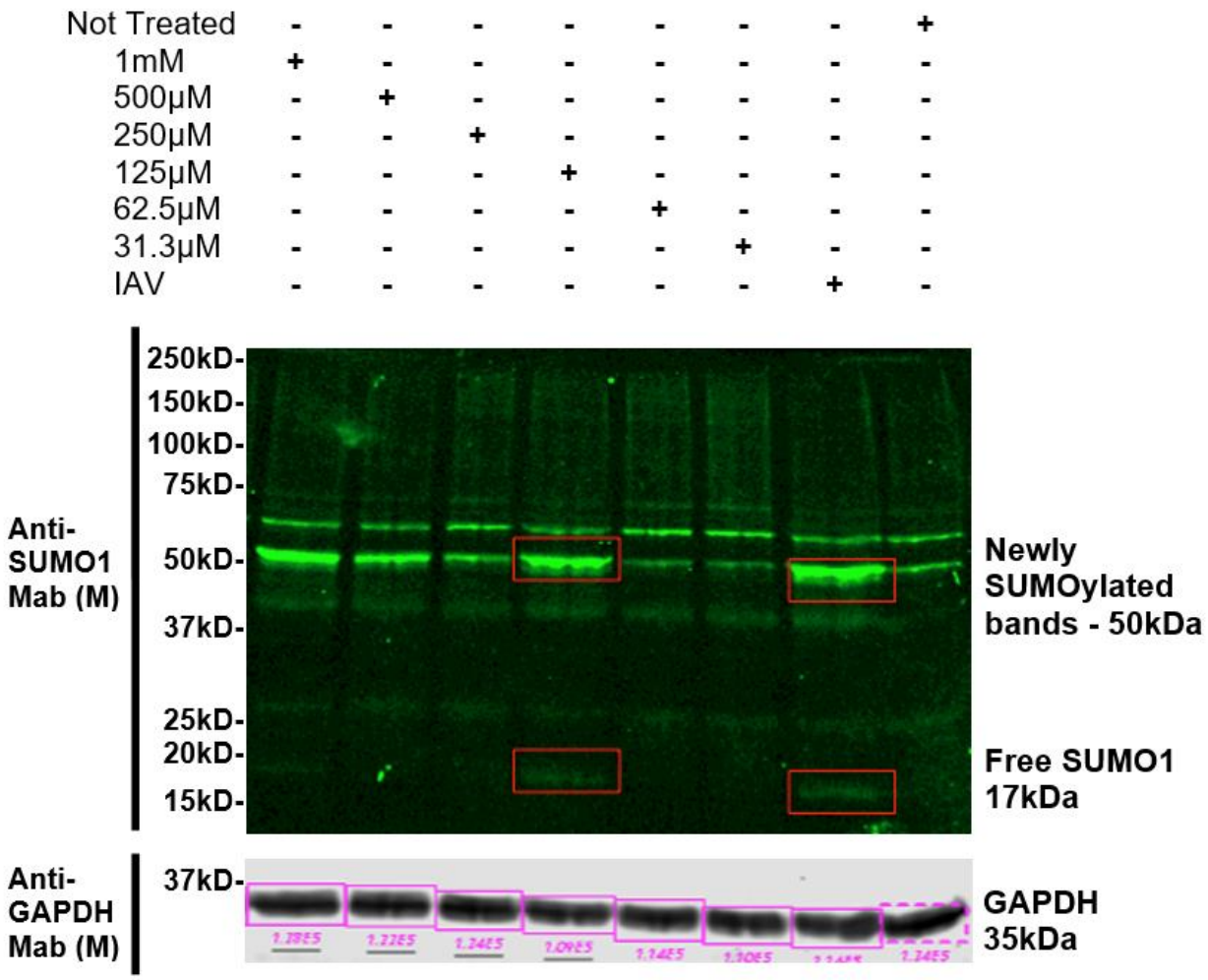

Figure 2.2 Inducing GICS of SUMO1 with the hypoxia model.

A549 cells were treated with doubling dilutions of Cobalt Chloride for 24 hours. The cells were collected and treated for analysis by SDS-PAGE and immunoblot. Treatment with 1mM CoCl2 did alter the SUMOylation profile, however the most dramatic change is seen in samples treated with 125µM. Increases in SUMOylation are seen at the 17kDa and 50kDa ranges. Changes in SUMOylation were compared to the positive control, Influenza infection (MOI:10 for 24 hours). Monoclonal antibodies (Mab) from rabbit (Rb) and mouse (M) were used to identify SUMO1 and GAPDH, respectively.

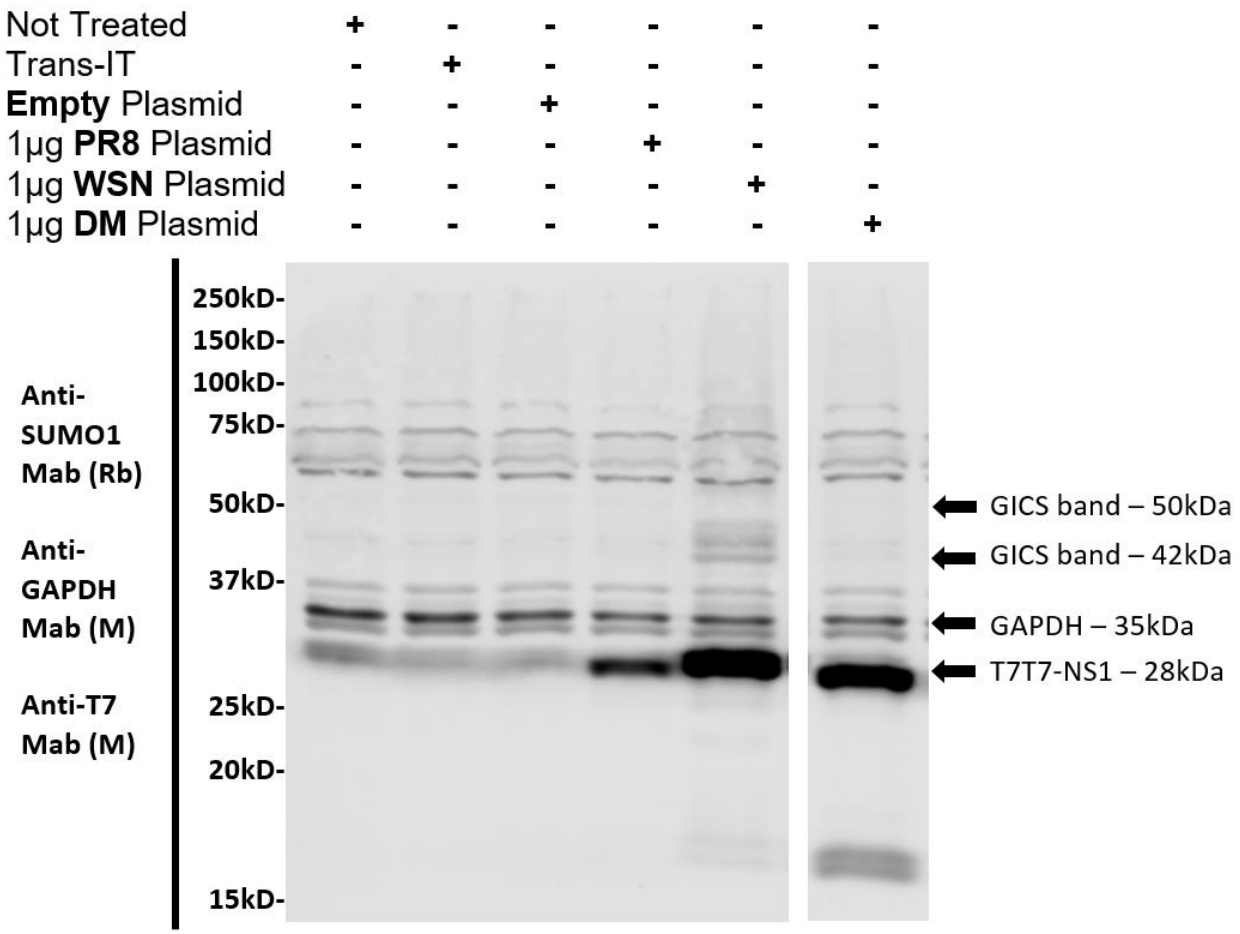

Figure 2.1 Validating GICS using NS1 from multiple strains of influenza.

A549 cells were transfected with gene segments coding for NS1 from different strains of influenza. 36 hours post transfection the cells were collected and treated for analysis by SDS-PAGE and immunoblot. Newly SUMOylated bands after transfection became present at the 40 and 52 kDa ranges. T7T7 tagged NS1 is synthesized in the samples transfected with NS1 from PR8, WSN, and the DM strains (lanes 4, 5, and 6). A change in the SUMO1 profile was seen with WSN but not as prominently with PR8 or non-SUMOylatable strains. The WSN strain of influenza will be used for infection experiments.

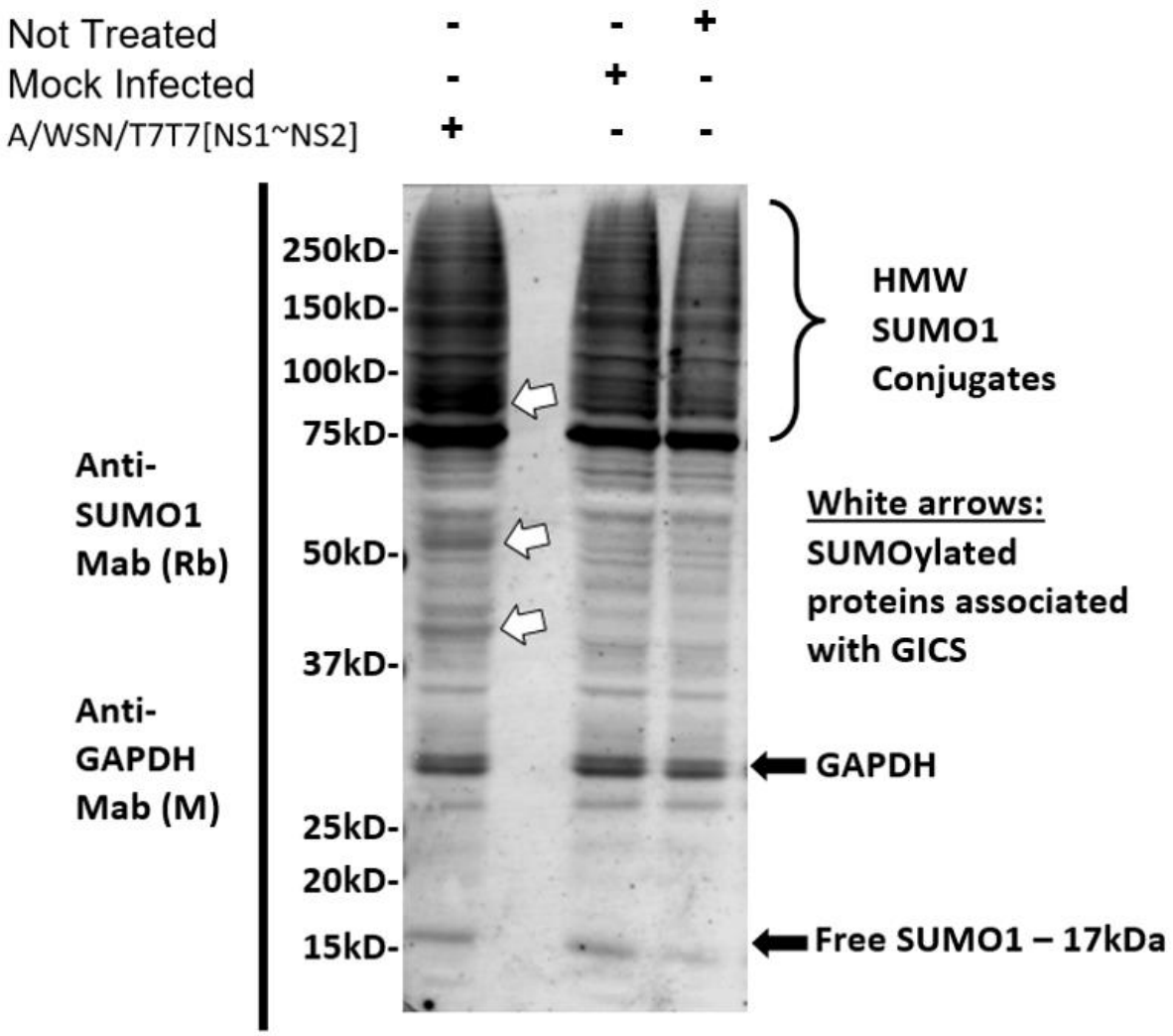

Figure 2.4 Inducing GICS of SUMO1 with the A/WSN/T7T7[NS1~NS2] strain.

A549 cells were infected with A/WSN/T7T7[NS1~NS2] at an MOI of 10 for 24 hours. The cells were collected and treated for analysis by SDS-PAGE and immunoblot. Non-infected and mock-infected cell extracts did not show changes in the SUMO1 profile. Virus infected cells present newly SUMOylated bands at the 40, 52, and 90 kDa ranges. High molecular weight (HMW) SUMO conjugates also appear in the WSN infected cell extracts and not as distinctly in the non-infected samples. Duration of infection will be optimized for optimal visualization of SUMO1 increases.

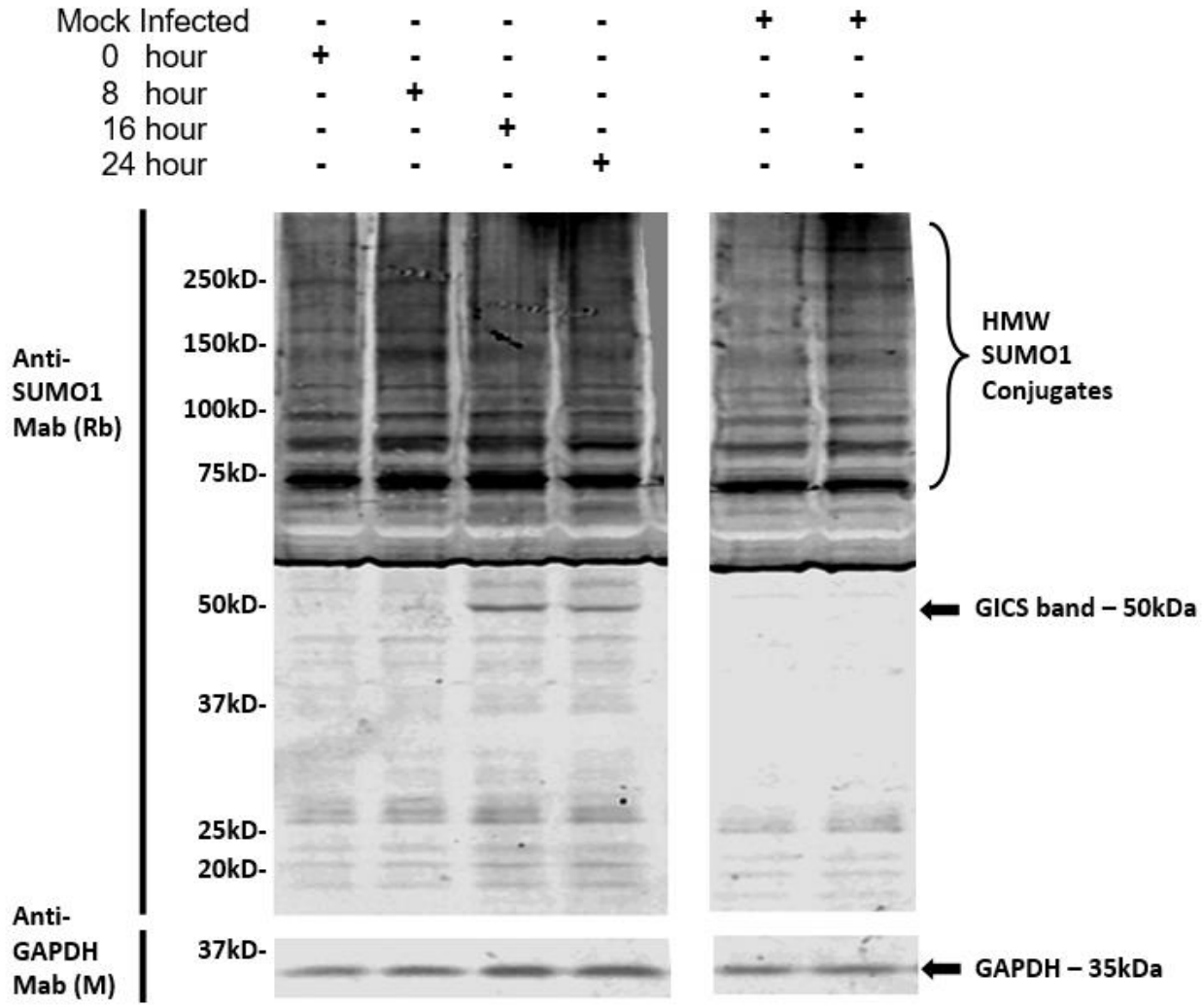

Figure 2.5 Time course optimization of the influenza infection model.

A549 cells were infected with A/WSN/T7T7[NS1~NS2] at an MOI of 10 for 24 hours. The cells were collected and treated for analysis by SDS-PAGE and immunoblot. Mock-infected cell extracts did not show changes in the SUMO1 profile. Infection for less than 8 hours did not result in any visible increases in the SUMO1 profile. Samples collected at the 16 and 24-hour time points showed newly SUMOylated bands present in the 42 and 50kDa ranges.

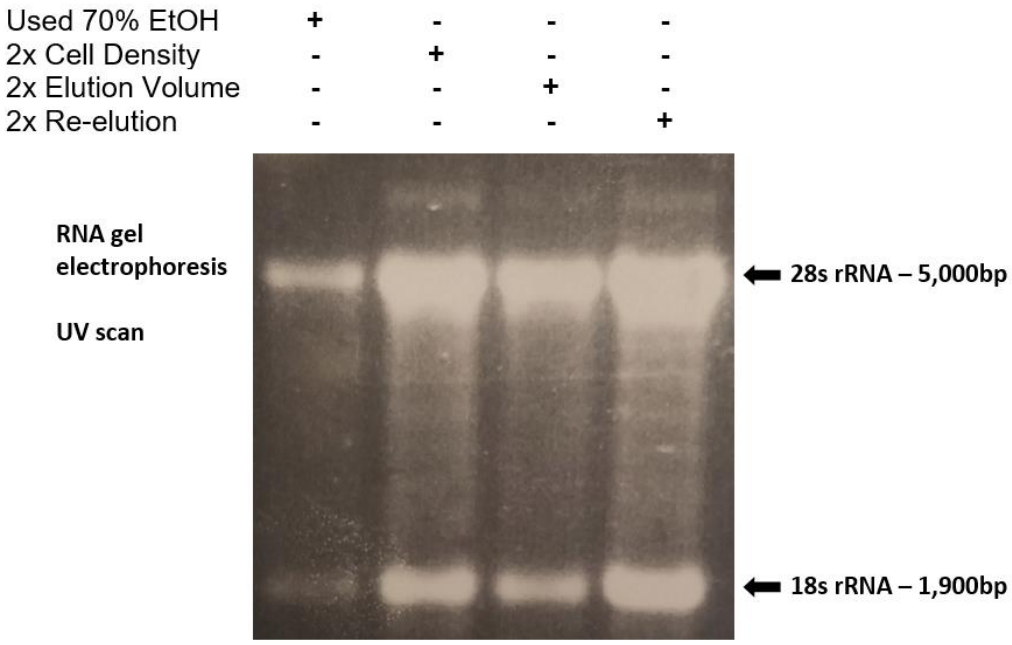

Figure 2.6 Total RNA elution and quantification.

Optimization of the elution process used in the final step of the RNeasy kit was performed. Using 70% ethanol made ahead of time resulted in decreased yield. Starting with twice the amount of cells than suggested resulted in yields similar to simply eluting the sample a twice using the same 30µL of QH2O. Using twice the volume, 60µL, to elute the RNA from the collection column resulted in a diminished concentration. After RNA extraction using the RNeasy kit, total RNA must be quantified. Prepared samples were resolved using formaldehyde agarose gel electrophoresis, visualized by UV light, and quantified by densitometry. 18s and 28s rRNA is visible at 1,900bp and 5,000bp, respectively, and used as a reference for total RNA. RNA concentration should be adjusted to uniform levels and further optimized for cDNA synthesis. RNA concentration was reverified by Nano-drop and 2µg of RNA was combined with 2.5µL of polyT primer [5µM] for optimal cDNA synthesis.

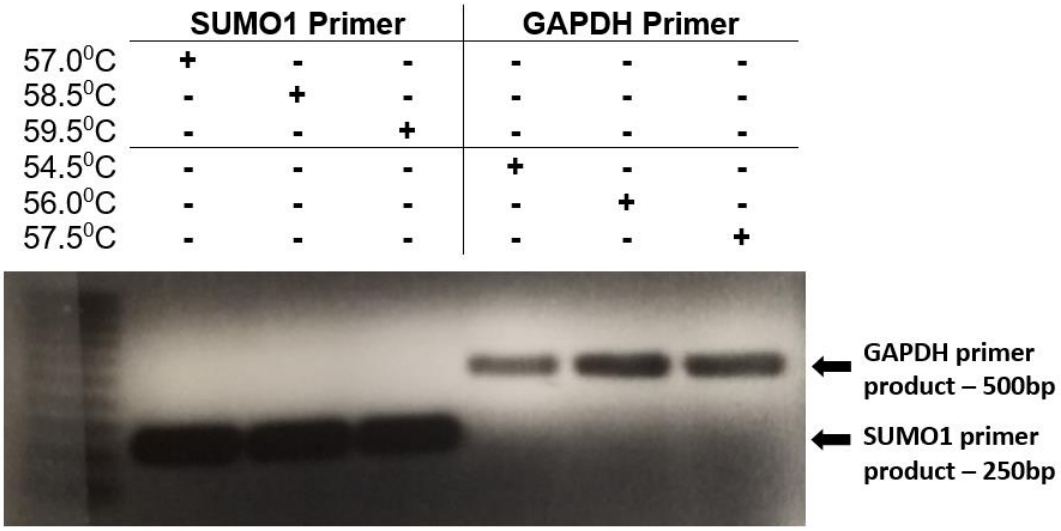

Figure 2.7 Primer annealing temperature optimization.

Prior to using the primers designed for the quantification of SUMO1 and GAPDH mRNA by qPCR, optimal annealing temperatures should be determined. Three temperature ranges for each primer was selected based on the primer's melting temperature and primers were incubated with TAQ-man polymerase and plasmids for either SUMO1 or GAPDH. The PCR product was resolved by DNA gel electrophoresis and visualized using Ethidium Bromide and exposure to UV light. The primers were designed to produce a 250bp double stranded product for SUMO1 and a 500bp product for GAPDH. The optimal temperature is 58.5^0C for SUMO1 and 56^0C for GAPDH. These temperatures will be used in future quantification experiments by qPCR and SYBR Green.

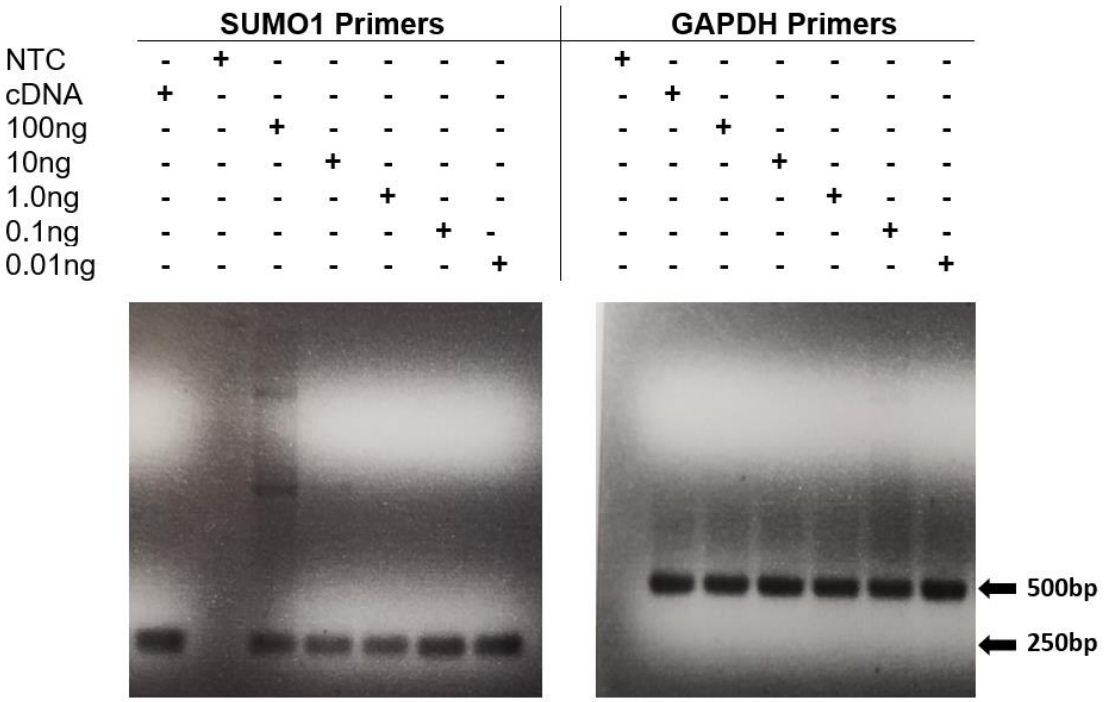

Figure 2.8 Final optimization and test of standards.

The SYBR Green polymerase was tested before use in the final qPCR experiment. The plasmid standards were also tested for proper dilution and PCR product. The No Template Control (NTC) returned no product after 30 cycles and was determined to be a functional negative control. The same cDNA was used for both SUMO1 and GAPDH primers also producing a correct sized product. The standards are serial dilutions of the plasmids coding for human SUMO1 and GAPDH. The standards will be used for absolute quantification of transcript copy number.

Table 2.1 Positive control validation.

To validate the settings used for RT-qPCR, an initial test was conducted using cells transfected to over express either a non-coding plasmid (empty) – #23, SUMO1 – #28, or GAPDH – #453. RNA was collected, quantified, and used for cDNA synthesis. The cDNA was then used for qPCR with SYBR Green. Using primers for either SUMO1 or GAPDH, cycles to threshold and absolute copy number were quantified. When SUMO1 transcripts for the positive control, SUMO1 transfected cells, were measured they had a decreased Ct value. Table 2.1A contains all qPCR values using the SUMO1 primers and table 2.1B is the quantification of GAPDH transcripts after transfection. No Template Control (NTC) and No Reverse Transcriptase (NRT) are negative controls and should not return any quantity values.

Table 2.1A – SUMO primers for qPCR

Sample	Cт	Cт Mean	Cт SD	Quantity	Quantity Mean	Quantity SD	Ct Thresh	Tm1
NTC	34.36						1.171	78.001
NTC	33.64						1.171	78.001
NTC	26.45						1.171	78.001
NRT	33.34	33.52	0.32	2.27E-08	1.99E-08	5.16E-09	1.171	78.001
NRT	33.32	33.52	0.32	2.31E-08	1.99E-08	5.16E-09	1.171	78.500
NRT	33.89	33.52	0.32	1.40E-08	1.99E-08	5.16E-09	1.171	78.500
#23	26.75	30.39	5.71	7.63E-06	3.90E-06	3.82E-06	1.171	77.997
#23	27.46	30.39	5.71	4.08E-06	3.90E-06	3.82E-06	1.171	78.499
#23	36.97	30.39	5.71	9.25E-10	3.90E-06	3.82E-06	1.171	78.499
#453	32.09	32.80	1.00	6.87E-08	4.42E-08	3.47E-08	1.171	78.499
#453	33.51	32.80	1.00	1.97E-08	4.42E-08	3.47E-08	1.171	77.997
#453	33.51	32.80	1.00	1.97E-08	4.42E-08	3.47E-08	1.171	77.997
#28	21.74	26.60	7.54	6.31E-04	2.94E-04	3.18E-04	1.171	77.997
#28	22.78	26.60	7.54	2.52E-04	2.94E-04	3.18E-04	1.171	78.499
#28	35.28	26.60	7.54	4.09E-09	2.94E-04	3.18E-04	1.171	78.499
Standard								
SUMO	8.28	8.282		100			1.171	77.501
SUMO	10.4	10.4		10			1.171	78.500
SUMO	13.48	13.48		1			1.171	78.500
SUMO	16.52	16.52		0.1			1.171	78.500
SUMO	18.28	18.28		0.01			1.171	78.500

Table 3.1B - GAPDH primers for qPCR

Sample	CT	CT Mean	CT SD	Quantity	Quantity Mean	Quantity SD	Ct Thresh	Tm1
NTC	37.04						0.365	86.001
NTC	31.95						0.365	87.502
NTC	32.51						0.365	87.502
NRT	34.68	35.37	0.62	7.25E-10	4.20E-10	2.68E-10	0.365	84.997
NRT	35.53	35.37	0.62	3.14E-10	4.20E-10	2.68E-10	0.365	86.001
NRT	35.89	35.37	0.62	2.21E-10	4.20E-10	2.68E-10	0.365	86.001
#23	28.47	31.18	2.66	3.24E-07	1.15E-07	1.81E-07	0.365	87.000
#23	31.30	31.18	2.66	2.00E-08	1.15E-07	1.81E-07	0.365	87.000
#23	33.79	31.18	2.66	1.74E-09	1.15E-07	1.81E-07	0.365	87.000
#453	21.68	26.41	5.07	2.55E-04	8.66E-05	1.46E-04	0.365	86.002
#453	25.80	26.41	5.07	4.45E-06	8.66E-05	1.46E-04	0.365	86.002
#453	31.76	26.41	5.07	1.27E-08	8.66E-05	1.46E-04	0.365	80.998
#28	25.01	29.02	5.18	9.70E-06	3.61E-06	5.30E-06	0.365	87.000
#28	27.19	29.02	5.18	1.13E-06	3.61E-06	5.30E-06	0.365	87.000
#28	34.87	29.02	5.18	6.03E-10	3.61E-06	5.30E-06	0.365	87.000
Standard								
GAPDH	8.66	8.66		100			0.365	86.501
GAPDH	10.35	10.35		10			0.365	86.501
GAPDH	13.45	13.45		1			0.365	86.501
GAPDH	16.50	16.50		0.1			0.365	86.501
GAPDH	17.30	17.30		0.01			0.365	86.501

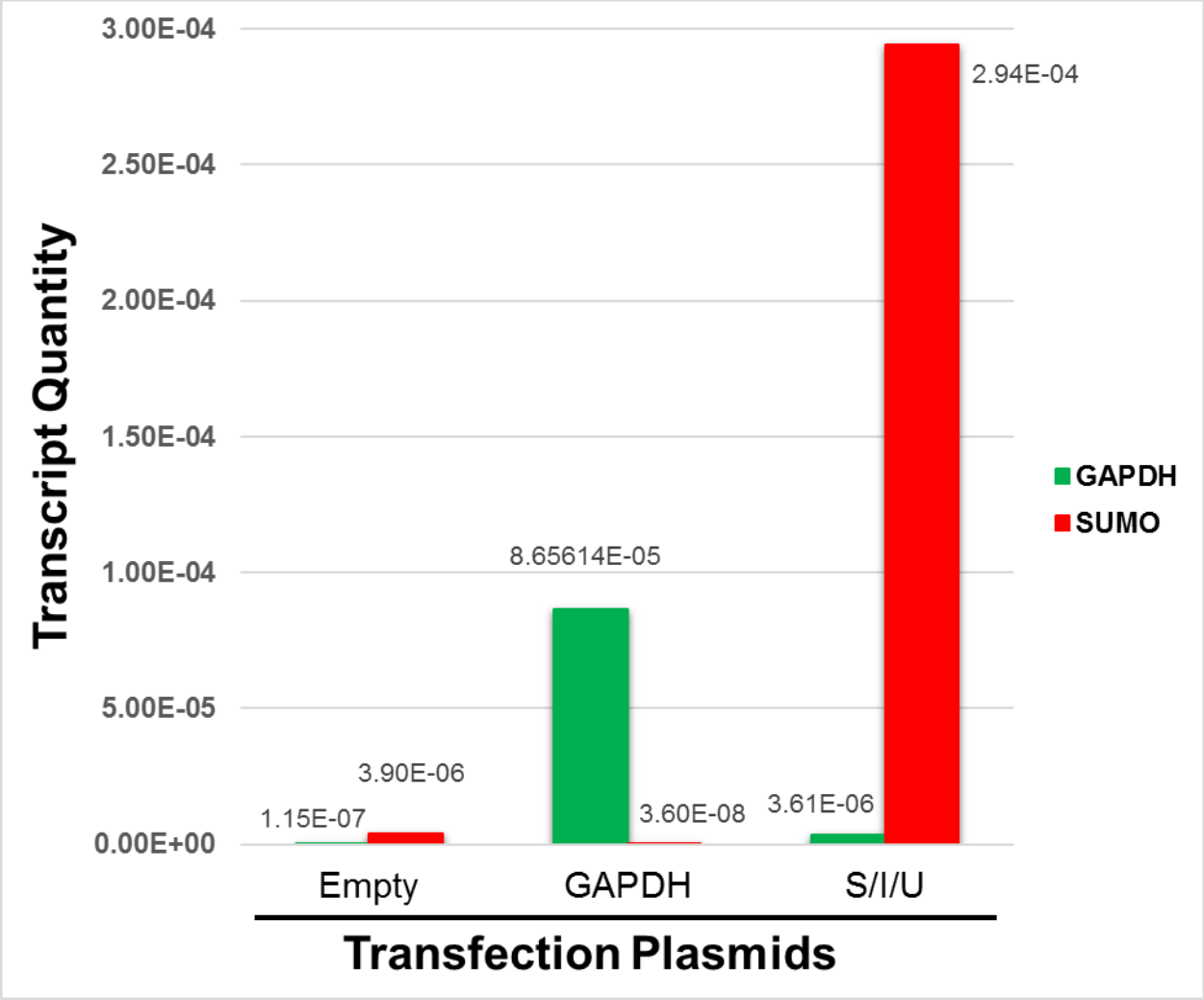

Figure 1.9 Validating qPCR sensitivity and component quality.

The mRNA measured in this experiment was extracted from cells transfected with either a non-coding plasmid (empty #23), GAPDH (#453), or a dual expression construct that causes a marked increase in cellular SUMOylation (#28). The non-treated control samples had very low basal levels of SUMO (red) and GAPDH (green) transcripts. After 36 hours of transfection with GAPDH or SUMO1/I/Ubc9 there was a dramatic increase in the number of transcripts present. This validates transfection, primer design, standards used for absolute quantification, and the SYBR Green kit for qPCR.

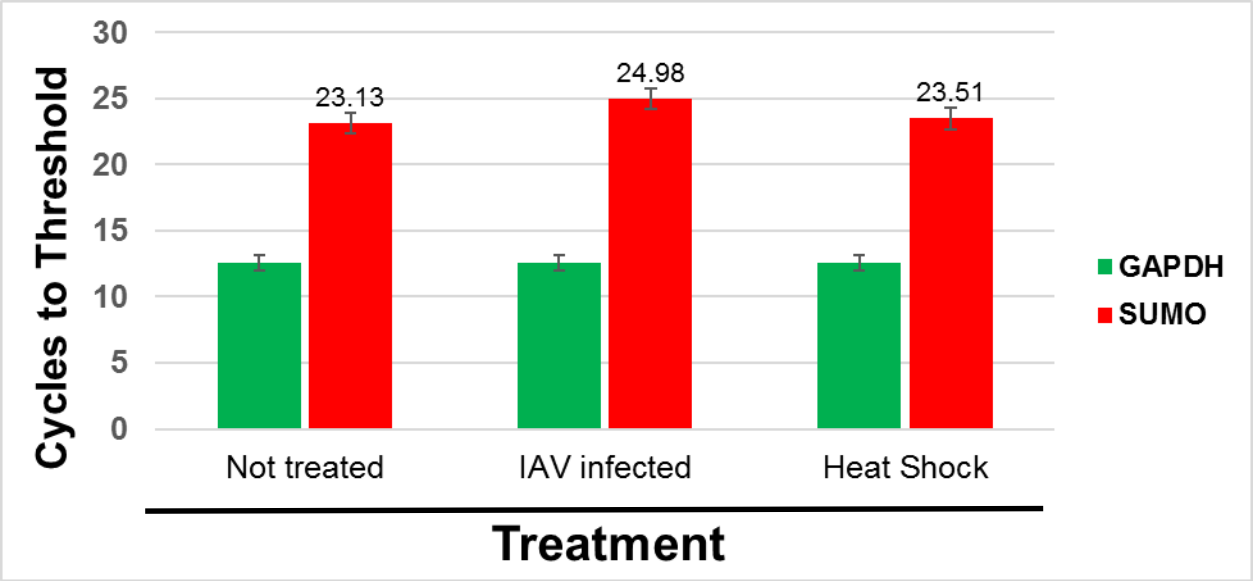

Figure 2.10A Number of cycles to reach threshold.

After 40 cycles, SUMO1 values were normalized to GAPDH. The IAV infected cells had fewer starting transcripts and had to undergo an average of 2 extra cycles to reach the threshold intensity cut off. The steady state levels of SUMO1 based on Ct values appear to be equal in the not treated and heat shock treated cells.

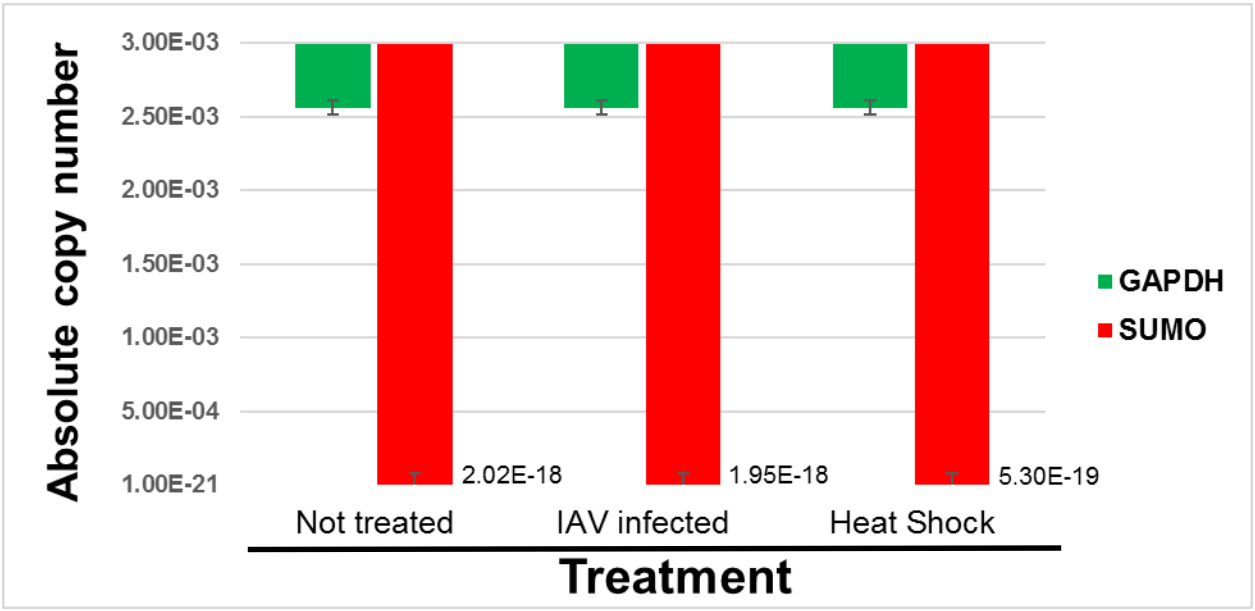

Figure 2.10B Absolute copy number.

Five serial dilutions of plasmid copies of known values were used as a standard to estimate starting transcript copy number. SUMO transcripts levels remain the same after influenza infection but decrease slightly after incubation at 420C for 45 minutes to induce heat shock.

2.4 DISCUSSION

Previous studies monitoring changes in SUMOylation as a response to cellular stress inducing factors such as heat shock, hypoxia, and influenza infection have suggested that the increases in SUMOylation are in some way protective. In the case of influenza infection, SUMOylation plays a large role in viral protein functionality. The primary focus of ongoing research is limited to the downstream effects of SUMO conjugation. How SUMO is regulated, activated, and targeted is not yet understood but could in fact be vital for the discovery of novel therapeutic measures that may enhance protective mechanisms currently utilized by the cell. Several studies have attempted to contribute the increases in SUMOylation seen by immunoblot to either a redistribution of SUMO from one set of proteins to a secondary set of proteins, or as a result of transcript regulation dictated by microRNA [Domingues et al. 2015; Sahin et al. 2014]. Here, we have optimized the necessary procedures required to accurately quantify steady state transcript levels from immortalized cell lines grown in tissue culture. This first stage of RT-qPCR has provided validation of technique and confirmed the results presented by other groups. To measure changes of SUMO transcript levels, the cells must undergo treatments which induce changes in SUMO that can be verified by immunoblot. The standardization of optimal conditions for each of the stress inducing models used to trigger Global Increases in Cellular SUMOylation (GICS) is followed by the optimization of RNA purification from the treated samples. The final stage of standardization involves the RT-qPCR components and procedures. Overall, this project has provided evidence that SUMO1 transcripts do not fluctuate as dramatically as do the corresponding proteins.

To ensure accurate and reproducible results, the conditions to induce Global Increases in Cellular SUMOylation (GICS) using each of the three models, heat shock, hypoxia, and influenza infection, require standardization. We demonstrate that by detaching adherent cells grown in tissue culture and submersing them in a water bath for 45 minutes, the cells undergo an adequate change in temperature which results in the activation of the cellular heat shock response as measured by a

marked increase in the SUMO1 profile. This protocol was modified from the cell line specific protocol detailed by Golebiowski and Hay et al. 2009. While the protocol effectively increases the time that the total population of cells are exposed to heat shock temperatures, detaching the adherent cells from the flask increases the amount of extraneous variables and potential loss of sample. The second stress model, cobalt chloride, was used to induce conditions that mimic hypoxia. Treating A549 cells with 125μM for 24 hours resulted in an increase in the SUMO1 profile similar to infection with influenza. Hypoxia, however, was not verified by the production of HIF-1α as the antibodies available did not target the correct species and further verification may be needed. The H1N1 WSN strain of influenza provided the most robust increase in SUMOylation and was used for the optimization of the infection model. Using a multiplicity of infection (MOI) of 10 viral particles per cell, an increase in the SUMO1 profile was seen after 16 hours but began to diminish after 24 hours. The increase in protein synthesis may not be a result of increased transcription but instead a consequence of increased translational activity of the transcripts present in the way of multiple ribosomes per transcript forming polysomes.

Following treatment, extraction and quantification of RNA for cDNA synthesis required optimization. Using the RNeasy kit to capture and elute RNA from tissue culture samples, the most efficient method that provides the maximum yield was to use 30μL of ultra clean water for the first elution and reuse the same volume for the second elution. This method dramatically increases the yield and minimizes error resulting from sample loss. The RNeasy kit is however a more expensive alternative to extract RNA and may have similar yet more uniform yields than using alternatives such as TRIzol. Two sets of primers were used in previous experiments to measure SUMO1 and GAPDH transcripts [Moore, 2013 and Schmittgen, 2000]. To ensure their validity and the conditions needed for these primers to function properly, several standardization steps were put into place. Annealing temperatures for each set of primers was determined through the use of a gradient of temperatures starting from below the calculated melting temperature. SUMO1

and GAPDH primers had similar annealing temperatures but require two different temperatures to be used for accurate results.

Overall, this project has standardized key procedural steps needed to increase reproducibility of the quantification of steady state transcript levels. The standards used to quantify transcript levels were created from serial dilutions of plasmids encoding SUMO1 or GAPDH from human origin. The positive controls were tested to show that the system was able to track changes in transcript levels for both sets of primers. The final RT-qPCR experiment provided evidence that steady state transcript levels of SUMO1 did not change as drastically as is seen in the protein profile.

Chapter 3: Regulation of the SUMO1 substrate targeting mechanism.

Changes in the SUMOylation profile are seen after exposure to several types of stress at both the cellular as well as the organismal level. A more detailed understanding of how these changes are regulated is vital for immune and stress response research. Protocols needed for the analysis of regulation at the transcriptional level were optimized in Aim 1 and following the standardization of protocols in Aim 2, SUMO1 conjugated proteins will then be able to be analyzed by mass spectrometry. In the attempt to detect SUMOylated proteins, two major issues arise. SUMOylated transcription factors are in very low abundance and are difficult to detect using traditional methods. Also, targets can easily be de-SUMOylated in non-denaturing conditions as SUMO isopeptidases remain highly active [Becker et al. 2013]. In attempt to overcome these obstacles, previous studies have attempted to identify all SUMOylated proteins by using artificially modified cellular environments. Proteins of interest are often overexpressed using either transiently expressed proteins (SUMO, Ubc9, or specific target proteins) or by stably expressing tagged versions of SUMO. The error in these methods is associated to the non-biologically accurate environment that is created by the artificial proteins and their resulting abundance [Barysch et al. 2014]. As a result, a research group has devised a method to enrich endogenously expressed proteins under denaturing conditions that is applicable for the analysis of the SUMOylated proteome [Becker et al. 2013]. The immunoprecipitation (IP) of SUMO1 will be accomplished by using hybridoma cells to produce high amounts of monoclonal antibodies at a low cost; this allows for the use of a very large quantity of antibodies to capture the total SUMO population including targets of very low abundance. The production of antibodies against SUMO1 through the use of hybridoma cells is a sub-aim and will require the culture of the cells and the inoculation of mice to form ascites. SUMO1 will then be immunoprecipitated and enriched from A549 cells using these monoclonal antibodies immobilized on protein G agarose beads. The target proteins will be further isolated by the introduction of an epitope spanning elution peptide specially designed to outcompete this interaction. The final pool of SUMO1 and its interacting partners will

be analyzed by mass spectrometry. The differentially conjugated set of proteins will be subdivided by function, and further analyzed in future studies.

3.1 MATERIALS AND METHODS

SUMO1 (21C7) hybridoma cell line:

The **21C7 anti-SUMO1** hybridoma cell line was developed by Dr. Michael J. Matunis from Johns Hopkins Bloomberg School of Public Health and obtained from the **Developmental Studies Hybridoma Bank at the University of Iowa**. The hybridoma cells were initially expanded from the 1mL vial received. To this end, the cells were thawed rapidly and supplemented with 50mL fresh media for a final concentration of 0.1% DMSO. The cells were pelleted at 3,000RPM for 5 minutes ensuring that the decelerate speed was at the lowest setting to not disturb the soft pellet that is formed by these suspension cells. The pellet was re-suspended in 15mL of complete medium consisting of **1x Roswell Park Memorial Institute medium (RPMI**) supplemented with high glucose, L- glutamine, sodium pyruvate **(Corning Incorporated Life Sciences, Corning, NY)**, and 10% **fetal bovine serum (Atlanta Biologicals, Inc., Flowery Branch, GA**). The T-25 flasks used to culture this volume of cells, and all flasks used to grow these hybridoma cells, should be maintained in a vertical orientation to facilitate proper oxygen exchange relative to surface area and cell density. Rock the cells gently on a daily basis to increase cell survival. If the cells are growing properly, 3 to 5 days later they will need to be expanded and can be transferred to a T-75. An equal volume of fresh media will be added to the T-75 to assist with the expansion of the culture. In approximately 7 days the culture will require a second expansion allowing for the required cell density to make a sufficient number of frozen stocks. Again, the volume should be transferred to a larger flask (T-175) and an equal volume of fresh media added. The final volume at this stage is 60mL and after one week can be increased to 120mL in a similar fashion while using the same flask. One week after this final expansion, frozen stocks should be made at $2x10^6$ cells/mL in a 1xRPMI + 10%FBS + 5%DMSO freezing solution.

BALB/c mice (Charles River Laboratories)

The mice were inoculated with 500µL of **Pristane (2,6,10,14-Tetramethylpenta-decane, Acros Organics**) 3 to 7 days prior to inoculation with the cell line via Intraperitoneal (IP) injection. Pristane is viscous and requires the use of both a larger needle (17-19g) and sedation by isoflurane. The sedation time is very short and is only needed to eliminate any movement by the mouse.

Preceding injection, the hybridoma cells must be sufficiently washed of Fetal Bovine Serum. This requires three washes of 50mL sterile 1x PBS each followed by a 5 minute and 3,000RPM spin. Before the final spin, cell density should be calculated. Following the removal of the final 50mL of 1x PBS, the pellet should be re-suspended in a final volume that brings the cells to a final concentration of $8x10^6$ cells/mL.

The mice were injected with approximately $4x10^6$ hybridoma cells in 500µL sterile 1xPBS by IP. Two to three weeks later, the mice usually reach the upper weight limit dictated by the IACUC and are sacrificed after collection of the ascites (the fluid is drawn from the abdominal cavity of the mice after anesthesia induced by isoflurane). Quantification and functionality tests, including SDS-PAGE followed by coomassie (protein concentration) and SDS-PAGE followed by immunoblot (functionality against target substrate), are subsequently conducted to verify concentration as well as functional dilution. Cell extracts containing enhanced levels of the substrate are used to measure functionality by immunoblot.

Both assays should be completed in 1-2 days after extracting the ascites and steps for long term storage should be taken. Before final storage, the antibodies need to be brought to a specific concentration, and also require the addition of two components. A final concentration of 50% glycerol and 0.05% sodium azide should be reached. This requires an adjustment of the antibody concentration from the initial concentration to the working concentration of 2mg/mL. Sodium azide can be added directly to this volume, accounting for the final volume which will be double the current volume. An equal volume of glycerol can then be added resulting in a final

concentration to be at 1mg/ml of antibodies, 50% glycerol and 0.05% sodium azide. Aliquots can be made at this time and must be stored at -20^{0}C.

Immobilization of antibodies:

8mg of monoclonal anti-SUMO1 was added to 1 ml of Protein G–agarose (Roche) equilibrated in 20mM NaH_2PO_4, pH 7.0. To cross-link the antibodies to Protein G, 50mM borate buffer, pH 9.0, containing 20mM dimethyl pimelimidate (DMP, Thermo Scientific) was freshly prepared and directly added to the agarose. After 1-hour incubation, the cross-linker was quenched with 50mM Tris, pH 8.0. Before use, beads were washed once with 200mM acetic acid, 500mM NaCl, pH 2.7, and twice with 20mM NaP, pH 7.0.

Transient transfections:

HEK293FT cells (Invitrogen Corp.) were seeded at a density of 3 x 10^5 cells/well into 6 well plates. 24 hours later, cells were transfected by liposome-mediated transfection using 5 µg of CsCl-purified plasmids and 15 µL of TransIT-LT1 (Mirus Bio LLC, Madison, WI) per well, according to the manufacturer's recommendations. Cells were incubated at 37^{0}C, 5% CO_2, for 36 hours. This incubation period was followed by the collection of cells for analysis by SDS-PAGE and immunoblot using 500µL of boiling 4x Sample Buffer (25 mM Tris [pH 6.8], 5% glycerol, 2% SDS, 0.01% bromophenol blue).

Plasmids:

pcDNA5/FRT/TO (Invitrogen) is a noncoding control plasmid and **pcDNA5/FRT/TO/SUMO1/IRES/HA-Ubc9 (developed by our lab)** allows for the dual expression of SUMO1 and, through an internal ribosomal entry site (IRES), the expression of Ubc9 at a lower abundance. This dual expression construct allows for increases in both SUMO1 protein levels and SUMO substrate conjugation.

Immunoblot analyses:

Before SDS-PAGE analyses, all cell extracts generated were passed several times through a 29½-gauge needle to break down the genomic DNA released and decrease the viscosity of the samples. Subsequently, β-mercaptoethanol was added up to a final concentration of 10%, and the samples were boiled for 5 min. The samples were resolved by 10% SDS-PAGE gels made in-house. Upon SDS-PAGE, the proteins were transferred onto **Immobilon-FL** (**Millipore Corp., Bedford, MA**) for use with **IRDye-conjugated secondary antibodies (LI-COR Biosciences Inc., Lincoln, NE)** and infrared fluorescence imaging.

Infrared fluorescence imaging:

Immobilon-FL membranes were washed 3 times in 1× PBS, blocked in Odyssey blocking buffer (OBB) (LI-COR Biosciences Inc.) for 1 hour at room temperature, and incubated in OBB supplemented with 0.1% **Tween 20** (here referred to as OBB-T) **(Thermo Scientific #233362500**) at 4°C overnight with the primary antibody at the indicated dilution. The membranes were then washed 3 times with 1× PBS-T and incubated for 1 h at room temperature in OBB-T with the appropriate highly cross-absorbed **IRDye 800 CW-** and **IRDye 680 LT-conjugated secondary antibodies (LI-COR Biosciences Inc.)** at the indicated dilution. The membranes were then washed 3 times with 1× PBS-T and twice again with 1× PBS and scanned on an Odyssey CLx infrared imaging system (LI-COR Biosciences Inc.). Quantitative analyses of the images obtained was performed by using Odyssey Infrared Imaging System Application software version 3.0.29 (LI-COR Biosciences Inc.).

Primary antibodies:

Rabbit Anti-SUMO1 (Y299 Abcam) and **Mouse anti-SUMO1 (ascites)** were both used at 1:3000 in Odyssey® Blocking Buffer (PBS) (LI-COR Biosciences Inc.) supplemented with 0.1% Tween20 (Thermo Scientific #233362500).

Secondary antibodies:

Both the IRDye 800 CW-conjugated goat anti-mouse IgG and the IRDye 680 LT-conjugated goat anti-rabbit IgG were used at a 1:20,000 dilution (LI-COR Biosciences Inc.).

Immunoprecipitation:

A549 cell line:

The alveolar cell line obtained from ATCC was maintained in complete medium consisting of 1x Dulbecco's modified eagle medium (DMEM) supplemented with high glucose, L-glutamine, sodium pyruvate (Corning Incorporated Life Sciences, Corning, NY), and 10% fetal bovine serum (Atlanta Biologicals, Inc., Flowery Branch, GA).

A549 cell lysate:

After exposure to treatment, A549 cells (8×10^6) were lysed in 8mL of lysis buffer (20mM sodium phosphate (NaH_2PO_4), pH 7.4, 150 mM NaCl, 1% SDS, 1% Triton, 0.5% sodium deoxycholate, 5mM EDTA, 5mM EGTA, 10mM NEM, 1 tablet of cOmplete Protease Inhibitor per 50mL (EDTA free - Roche Life Science). NEM is needed to inhibit the isopeptidases responsible for deSUMOylation. The viscous lysate was sonicated until it became fluid. The cell lysate was then supplemented with 50 mM dithiothreitol (DTT), boiled for 10 min and finally diluted 1:10 with RIPA buffer **without SDS** (20mM NaP, pH 7.4, 150 mM NaCl, 1% SDS, 1% Triton, 0.5% sodium deoxycholate, 5mM EDTA, 5mM EGTA, 1 tablet of cOmplete Protease Inhibitor per 50mL, and 20mM NEM). The lysate was filtered through a 0.45-µm filter (Rotilabo syringe filters, Carl Roth GmbH) and used for immunoprecipitation.

Immunoprecipitation and peptide elution:

For SUMO1 immunoprecipitation, 100 µL immobilized antibodies were added to the 10 ml of lysate and incubated overnight at 4 °C. Beads were washed three times with 20mM NaP, pH 7.4, 150mM NaCl, 0.1% SDS, 1% Triton X-100, 0.5% sodium deoxycholate, 5mM EDTA, 5mM EGTA, 10mM NEM, and 1 tablet of cOmplete Protease Inhibitor per 50mL. A final wash with three bead volumes of high-salt buffer (500mM NaCl instead of 150mM) was carried out for 30 min at 37°C on a rotating wheel. Two consecutive elution steps were performed at 37 °C on a rotating wheel for 30 min, each time using three bead volumes of elution buffer (high-salt buffer plus 0.5 mg/ml epitope-containing peptide (for SUMO1 21C7, VPMNSLRFLFE - GenScript). Stock solutions of 10 mg/ml in DMSO were stored at –80 °C. Immunoprecipitation efficiency will be measured by SDS-PAGE and sent for analysis by Mass Spectrometry.

3.2 RESULTS

Hybridoma cells:

Efficient synthesis of high quality antibodies requires implementing quality control checkpoints so as not to jeopardize thousands of hours and dollars. The first checkpoint verifies if the hybridoma cells are indeed synthesizing the correct antibodies and if the antibodies are able to recognize the intended substrate. An initial screening using 5mL of tissue culture supernatant supplemented with polysorbate20 to a final concentration of 0.1% was used in place of primary antibodies (**Fig. 3.1**). The supernatant contained antibodies against SUMO1 and were detectable by anti-mouse secondary antibodies. The large volume needed to visualize the substrate, SUMO1, provides evidence that the antibody concentration is low and will need to be concentrated or synthesized in an alternative manner. Free His-SUMO1 seen at 20kDa and SUMOylated RanGAP (80kDa) are the two main proteins that increase after transfection with this construct. The cells over-expressing SUMO1 showed to have a marked increase in signal greater than the cells

transfected with an empty plasmid or a plasmid designed to overexpress SUMO2. The antibodies were produced in tissue culture, are fully functional, and were not cross-reactive with other cellular proteins.

Ascites test:

The concentration of the antibodies present in the ascites fluid collected from balb/c mice must be determined. This was accomplished by diluting, treating, and resolving the samples by SDS-PAGE followed by Coomassie stain (**Fig. 3.2**). The samples primarily contain two proteins. After exposure to the denaturing conditions used for SDS-PAGE sample preparation, IgG is visible in two distinct ranges, 25kDa (Light chain) and 50kDa (Heavy chain). The second protein, albumin, is present at 65kDa. Bovine Serum Albumin (BSA – 65kDa) was used to create a standard curve for the quantification of the antibodies. The 7mL of ascites, collected from one mouse, contained 10mg/mL of antibodies, for a total of 70mg.

Anti-SUMO1 IgG functionality test:

After determining concentration, the antibodies derived from balb/c mice were tested for functionality. This assay not only determines functionality but also compares recognition of the substrate to a commercially available antibody against SUMO1 (**Fig 3.3**). Cells were transfected with the dual expression construct SUMO1/IRES/Ubc9, treated for SDS-PAGE and analyzed by immunoblot. Transfer membranes were incubated overnight with antibodies against SUMO1 [1µg/µL] at a dilution of 1:3000 (left: antibodies from Abcams – right: antibodies from hybridoma cells). When used at the same concentration, commercially available antibodies against SUMO1 did not compare to the hybridoma based antibodies; as determined by a decrease in specificity seen in lane 3 **(free SUMO1 at 20kDa**) and a decrease in sensitivity (**lanes 1 and 2**). The membrane incubated with hybridoma antibodies had a SUMO1 signal that is more prominent while background noise is noticeably decreased. For future experiments involving the detection of

SUMO1, the hybridoma derived anti-SUMO1 IgG is the better option to eliminate potential cross reactivity. In addition, the hybridoma derived antibody's epitope has been mapped and an epitope spanning peptide has been developed to be used to outcompete the interaction with SUMO1, ultimately allowing for the detachment of SUMO after immunoprecipitation.

Antibody saturation:

The theoretical total amount of SUMO1 that can be captured by each anti-SUMO1 IgG is estimated as a molar ratio of 2 SUMO1 proteins per 1 antibody. This was verified by incubating a constant amount of anti-SUMO1 with increasing concentrations of purified SUMO1 protein for 1 hour at 4^0C on a hula shaker. Saturation of the antibodies was determined by immunoprecipitation, SDS-PAGE, and Coomassie. The 2µg of antibodies against SUMO1 were able to capture a maximum of 1µg of purified SUMO1 at which point saturation was reached as determined by the plateau in fluorescence (**Fig 3.4A**). SUMO1 seen at 17kDa was quantified and the fluorescence intensity is shown in graphical from (**Fig 3.4B**).

Crosslinking the antibodies to protein G–agarose:

Crosslinking was performed to further optimize the immunoprecipitation process. By immobilizing the antibodies on beads, the final samples will not be contaminated with an excess of antibodies against SUMO1. Following the quenching step in the crosslinking process, the antibodies were tested for crosslink efficiency. The antibody/bead eluate was incubated at 37^0C for 30 minutes and then centrifuged to obtain two fractions. Each fraction was then treated for SDS-PAGE and analyzed by Coomassie stain. The optimal result of this process should provide a pellet fraction that contains antibodies fixed on beads and a supernatant fraction with little to no antibodies. Crosslinking did result in a supernatant fraction with minimal antibodies seen at 25 and 50kDa (**Fig 3.5A**). The non-crosslinked antibody samples, however, released a large amount of

antibody into the supernatant fraction. The pellet and supernatant fractions were quantified and compared in **Fig 3.5B.**

Final immunoprecipitation optimization:

To ensure optimal results, a final immunoprecipitation trial was performed using transfected cell extracts. HEK293FT cells were transfected with the dual expression construct SUMO1/IRES/Ubc9 to induce increases in free and conjugated SUMO1. Samples were saved from each step to verify efficiency of the entire process. Input refers to the starting cell extract not yet exposed to antibodies and should contain the most dilute concentration of SUMO1 (**Fig 3.6 lane 1**). Cell extracts were then incubated with the crosslinked antibodies on a hula shaker for 1 hour at 4^0C. This was followed by centrifugation that produced two fractions. The supernatant was saved and used to determine the quantity of SUMO1 that was not captured during the incubation period (**Fig 3.6 lane 2**). The pellet which captured SUMO1 and its interacting partners was then washed to eliminate non-specific binding – pre elution wash (**Fig 3.6 lane 3**). The pellet was incubated with epitope spanning peptides to outcompete with the interaction taking place between SUMO1 and the antibodies. This allowed for the release of SUMO1 and binding partners into the supernatant. At this stage, the pellet only contains antibodies crosslinked to beads and was saved for reuse. The supernatant eluate contains a high concentration of SUMO1 and could be used for further analysis by mass spectrometry (**Fig 3.5 lane 4**). All samples were treated for SDS-PAGE and analyzed by immunoblot. Anti-SUMO1 (Rb) was used with goat anti-Rabbit secondary antibodies to visualize changes in SUMO1 while goat anti-Mouse secondary antibodies bound directly to residual hybridoma derived antibodies. The total amount of SUMO1 present in the transfected cell extracts was outside of the range capturable by this quantity of antibodies and should be taken into account for experiments involving increases in SUMO1 (**Fig 3.6 lane 2**). Immunoprecipitation using antibodies targeting SUMO1 resulted in the enrichment of both endogenous SUMO1 and the transfected His-SUMO1 in the final eluate. Secondary antibodies

that target mouse proteins revealed that a small fraction of antibodies remained in the final eluate as seen at 25kDa and 50kDa for the light and heavy chains, respectively (**Fig. 3.6 lane 4 – lower image**). The higher molecular weight bands present are most likely antibody aggregates (75kDa and 150kDa) that did not fully denature during treatment for SDS-PAGE.

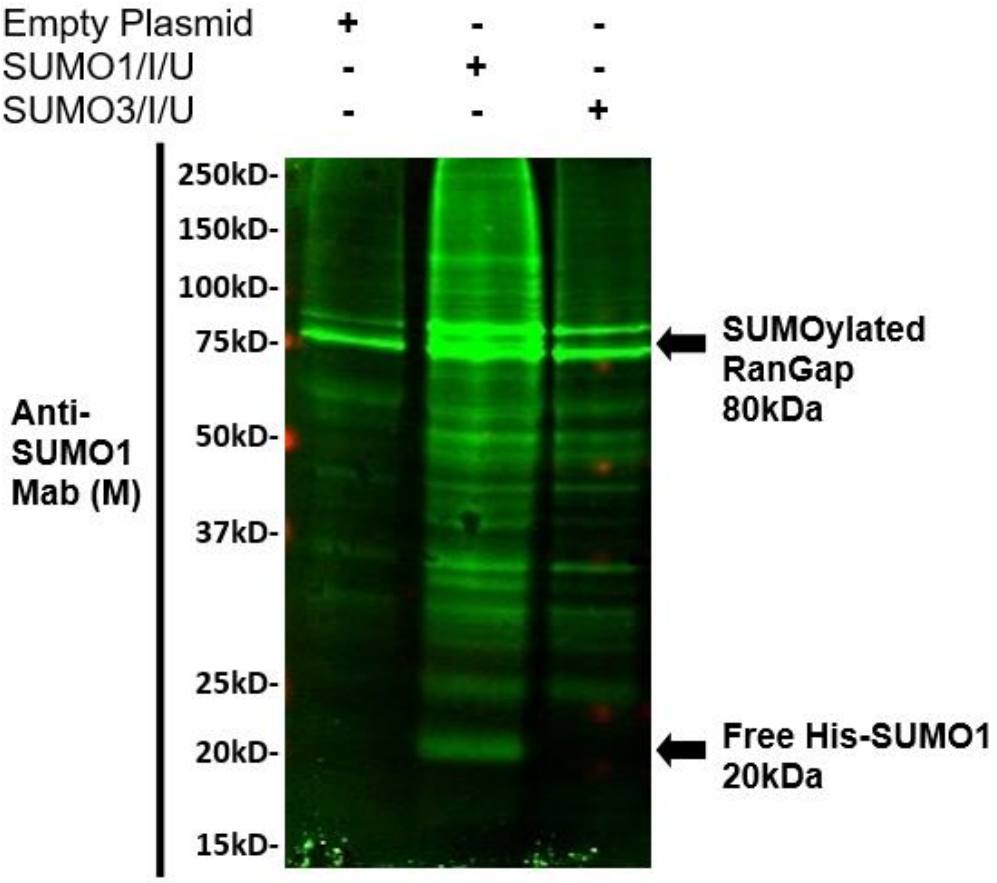

Figure 3.1 Hybridoma cell functionality assay.

Prior to the inoculation of balb/c mice with hybridoma cells that produce antibodies against SUMO1, they must be tested for IgG production. Supernatant from hybridoma cells grown in cell culture was tested for the presence of functional antibodies. HEK293FT cell extracts transfected with either a non-coding plasmid, a dual expression construct coding for SUMO1, or SUMO2 were resolved by SDS-PAGE and analyzed by immunoblot. The supernatant was supplemented with polysorbate20 to a final concentration of 0.1% and used as the primary monoclonal antibody (Mab) derived from a mouse (M). The membrane was then probed with goat anti-mouse antibodies with flourophores excitable at 800nm. Free His-SUMO1 seen at 20kDa and SUMOylated RanGAP (80kDa) are the two main proteins that increase after transfection with this construct. The cells overexpressing SUMO1 showed to have a marked increase in signal while the cells overexpressing the other two plasmids did not. The antibodies were fully functional and were not cross-reactive with other cellular proteins.

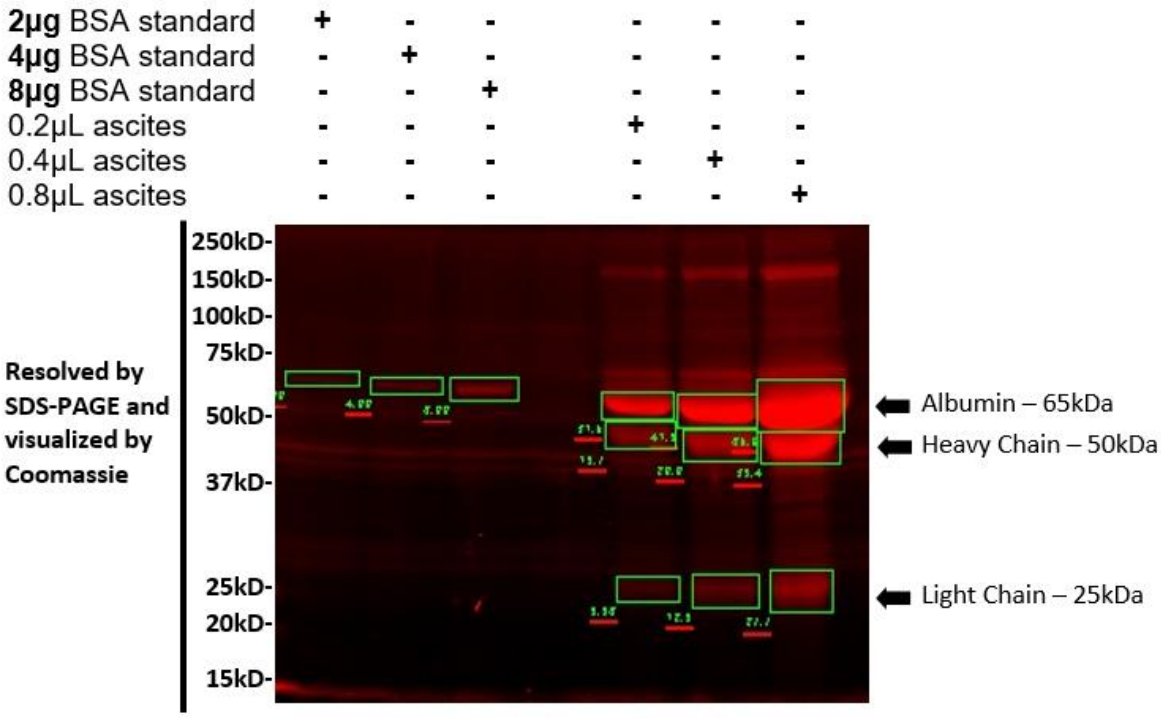

Figure 3.2 Quantification of SUMO1 IgG from ascites.

The ascites fluid was collected from balb/c mice inoculated with hybridoma cells that produce antibodies against SUMO1. This fluid with a high concentration of anti-SUMO1 IgG was diluted 1:10 and then treated for analysis by SDS-PAGE. This was followed by Coomassie stain and visualized 680nm. The BSA standard was used to calculate IgG concentration. The heavy chain domain of the denatured antibody was used to calculate total concentration and the volume was adjusted to 2µg/µL before adding an equal volume of 100% glycerol. This final volume was supplemented with sodium azide to a final concentration of 0.05%, aliquots were made and stored at -200C.

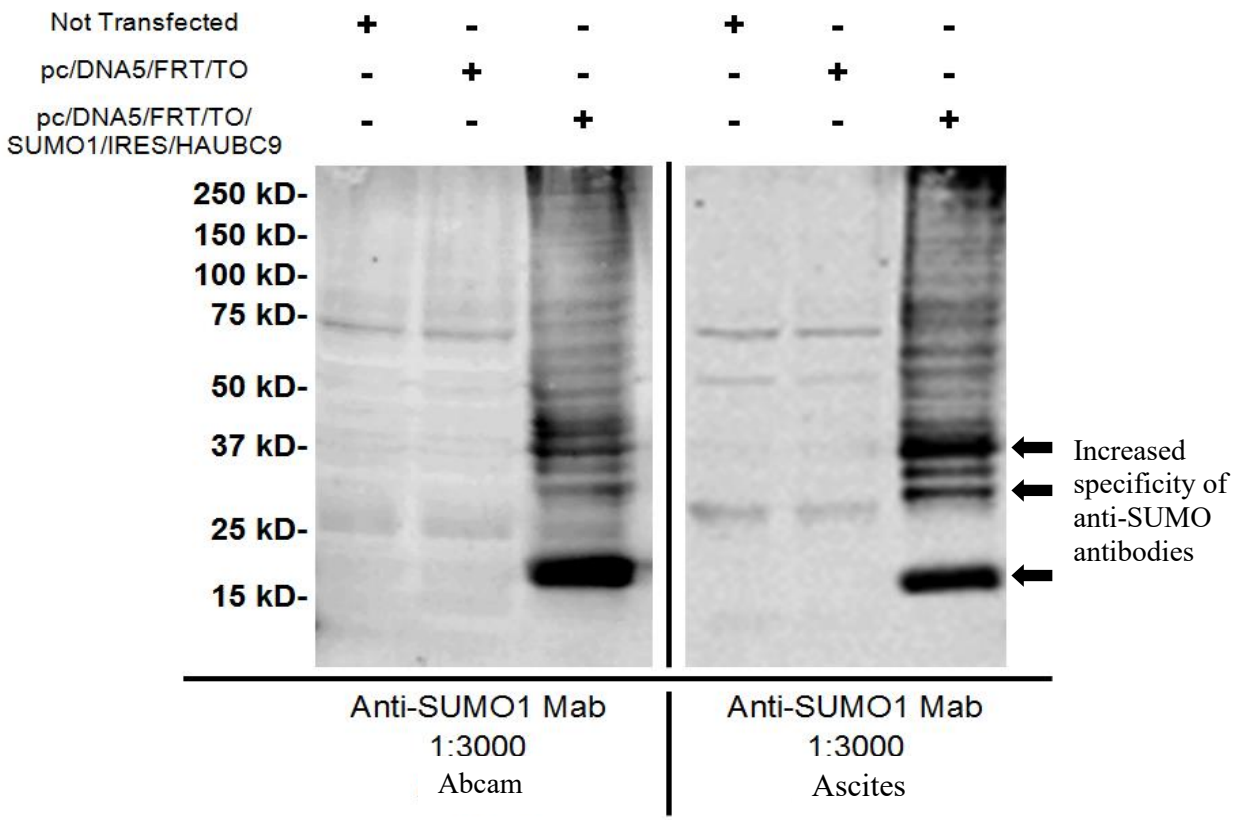

Figure 3.3 Comparison of hybridoma derived SUMO1 antibodies.

The SUMO1 antibodies currently available from commercial sources when compared to the anti-SUMO1 IgG produced by hybridoma cells do not possess the specificity or sensitivity needed for immunoprecipitation assays. HEK293FT cell extracts were collected after transfection i) Not treated, ii) empty plasmid (pcDNA5/FRT/TO), or iii) pcDNA5/FRT/ TO/SUMO1/IRES/HA-Ubc9. Transfer membranes were incubated overnight with antibodies against SUMO1 [1µg/µL] at a 1:3000 dilution (left: antibodies from Abcam – right: antibodies from hybridoma cells). Unconjugated SUMO is seen near 20kDa. At a final concentration of 0.3ng/µL the SUMO1 collected from the ascites had increased levels of specificity, as seen by the increase in the intensity of SUMOylated bands (lane 3). They also exhibit an increase in sensitivity as seen by the decrease in background bands lane 1 and 2.

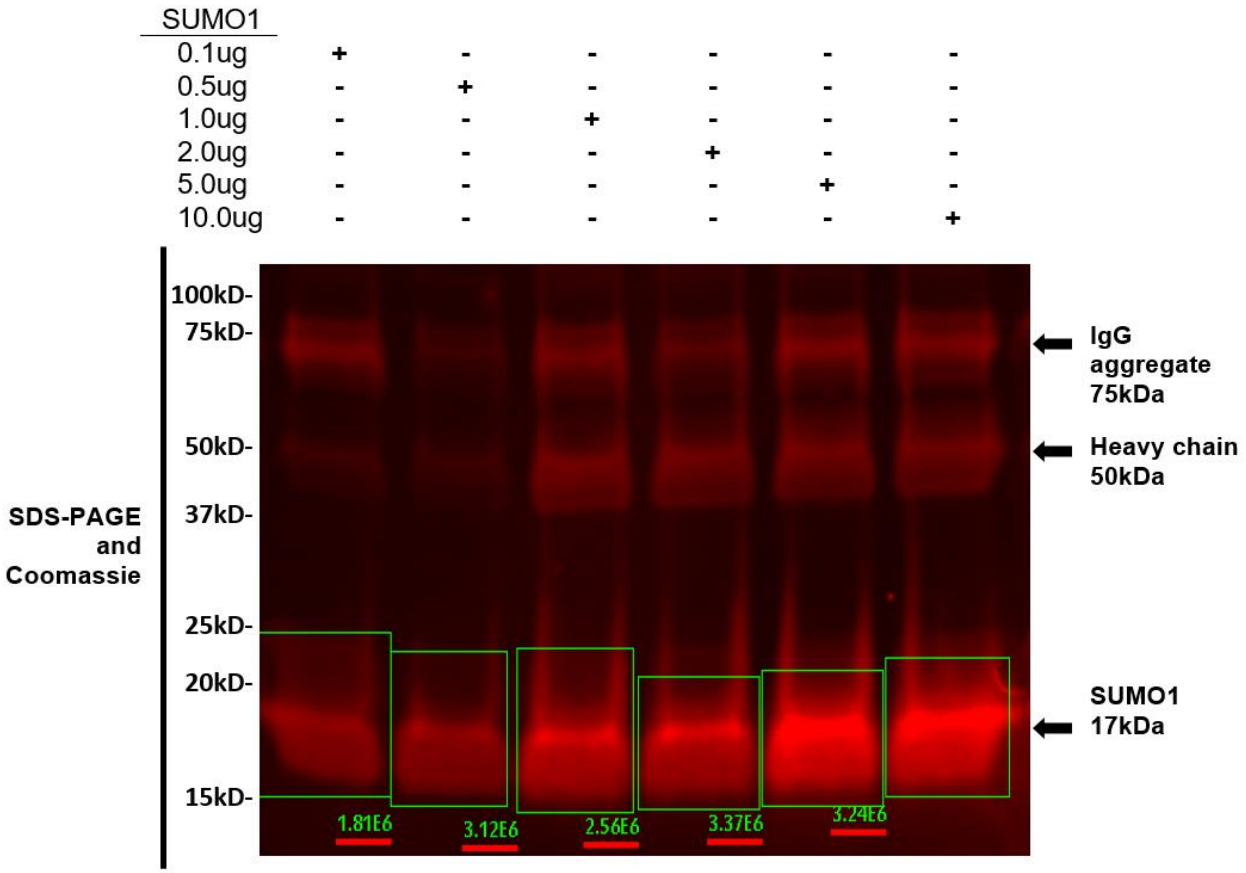

Figure 3.4A Antibody saturation.

Saturation of hybridoma derived antibodies by SUMO1 was determined by immunoprecipitation. Increasing concentrations of purified SUMO1 protein were incubated with 2µg of antibodies against SUMO1. The percipitate was analysed by SDS-PAGE and Coomassie stain. Saturation, determined by the platue of fluorescence intensity at 680nm, was reached with 1µg of SUMO1 (17kDa). IgG is visible at 50kDa for the heavy chain and 75kDa for the heavy and light chain.

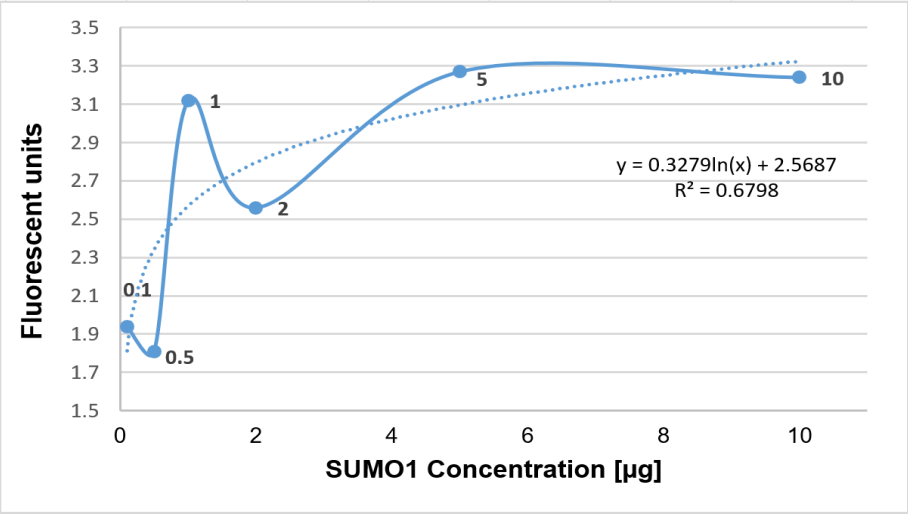

Figure 3.4B Antibody saturation quantification.

The fluoresence intensity of SUMO1 captured by immunoprecipitation is presented in this figure. The saturation of IgG is reached with 1µg of SUMO1. The experimental sample containing 2µg of SUMO1 shows a marked decrease in fluoresnece, this was due to experimental error as the following two concentrations displayed similar values as the 1µg sample. Data was plotted and a logarithmic trendline determined by using Microsoft Excel (2010).

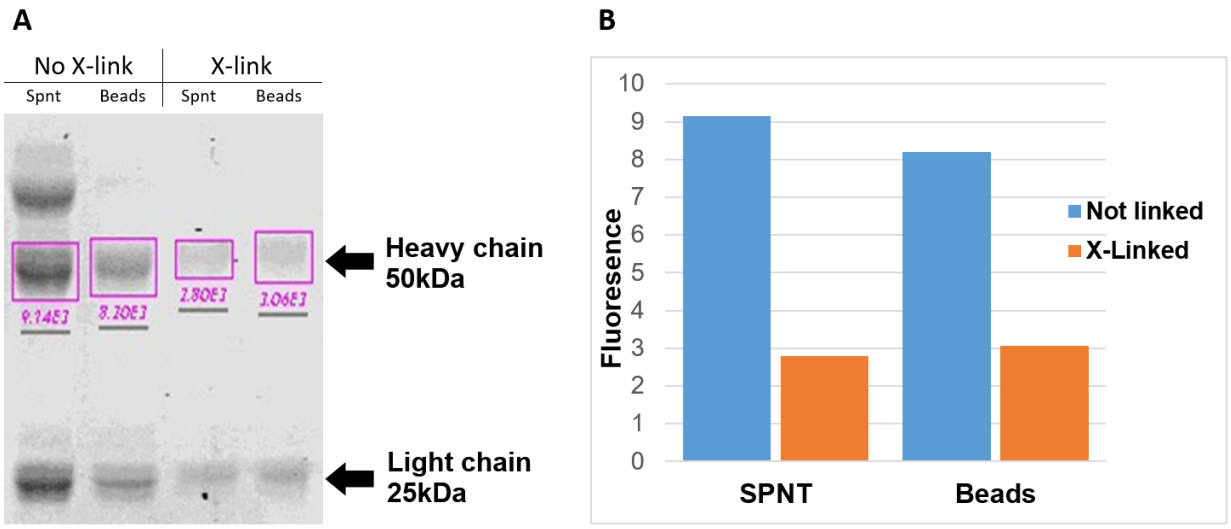

Figure 3.5 Crosslinking optimization.

Immunoprecipitation purity is ensured by crosslinking the antibodies to beads. After crosslinking, the samples were incubated at 37^0C for 30 minutes and then centrifuged to obtain two fractions - a pellet of antibodies cross-linked to beads and the supernatant (SPNT) fraction. To determine crosslink (X-link) efficiency, the samples were treated for SDS-PAGE and Coomassie analysis. The amount of antibodies that became detached from the beads, and were found in the supernatant after the 37^0C incubation period were much higher in the non-crosslinked samples when compared to the ones that did undergo crosslinking.

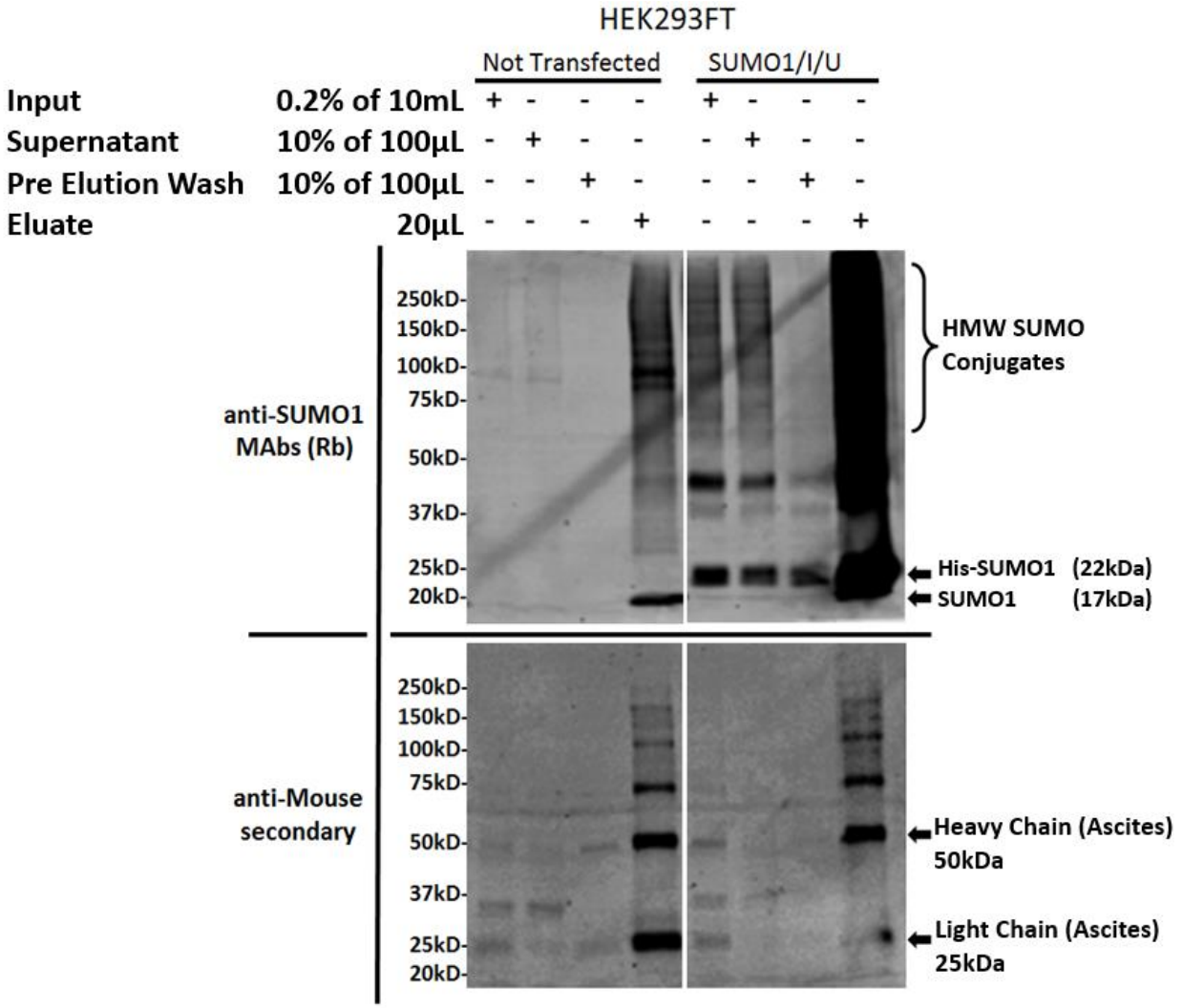

Figure 3.6 Final optimization.

The immunoprecipitation optimization was performed on two cell extracts. HEK293FT cells were either not treated or transfected with a dual expression construct to overexpress SUMO1 and Ubc9. The final eluate was resolved by SDS-PAGE and visualized by antibodies against SUMO1. Increased levels of SUMO require a higher concentration of antibodies to capture the entire population of SUMO1. The supernatant from the immunoprecipitation of transfected cell extracts contained high amounts of SUMO1 that was not captured and will affect further analysis. Following immunoprecipitation, endogenous SUMO1 (17kDa) is enriched under both settings but the high amount of His-SUMO1 (22kDa) in the transfected samples makes it difficult to visualize.

3.3 DISCUSSION

Previous groups have attempted to conduct full proteomic analyses to determine which proteins are modified by SUMO under several conditions and in different cell lines. Data from those groups have decreased reliability because they were using exogenous additives to render the changes measurable. The results from projects altering protein structure or synthesis rate will create new and immeasurable downstream effects on an unknown set of processes. To date, no other research has shown which proteins are SUMO modified after influenza infection using endogenous SUMO1. Immunoprecipitation coupled with peptide elution will provide the most accurate and biologically relevant insight into the changes that take place in the targeting of SUMO1 after infection and stress. The work presented here includes a detailed account of standardized protocols required to obtain maximal efficiency and reproducibility. A high concentration of antibodies against SUMO1 is required to conduct multiple replicates and ensure high yields of protein for analysis by mass spectrometry. The most efficient and cost effective means to acquire the necessary amount of antibodies needed is to use hybridoma technology. The hybridoma cells created by Dr. Michael Matunis at Johns Hopkins University were mapped by the Melchior group and they designed peptides that span the entire epitope to out compete the antibody substrate interaction. The use of this technology provides a large amount of highly effective antibodies that can easily be removed from the target protein, ultimately increasing sample purity and overall accuracy of the experiment. The data derived though using these standardized and optimized protocols will add to our understanding of how SUMO1 is regulated at the protein level and which proteins are preferentially targeted after exposure to stress.

Three major requirements for a successful immunoprecipitation: *i)* a large quantity of functional antibodies that target the substrate of choice and have little to no cross-reactivity with other cellular proteins *ii)* treating the cells to induce stress, described in chapter 2 *iii)* collecting the cell extracts under denaturing conditions to ensure that no de-SUMOylation occurs. To address the antibody requirements, the media used to grow the hybridoma cells in tissue culture was tested

for presence, functionality, and specificity of the IgG. The cells were indeed producing high amounts of quality antibodies targeting SUMO1. Balb/c mice were injected, via IP, with the same cells and the ascites fluid that developed contained high concentrations of anti-SUMO1 IgG. The antibodies were then compared to commercially available antibodies from ABCAM. When used at equal concentrations, the hybridoma antibodies were found to have enhanced specificity and sensitivity. Two quality control steps were completed prior to the use of these antibodies in the final immunoprecipitation. First, the antibodies were tested for saturation. The molar ratio of antibodies to substrate was estimated to be 1:2. This was tested by the immunoprecipitation of increasingly saturated antibodies. The final results demonstrate that 2µg of antibodies are fully saturated with 1µg of purified SUMO1. This quality control step allowed us to verify if the antibodies were indeed able to be used for immunoprecipitation as well as to identify the saturation point that will assist in the calculation of total amount of antibodies needed for future experiments. Second, the antibodies were chemically crosslinked to protein G agarose beads which increases sample purity by limiting the total amount of antibody loss.

Overall, this project has set into place crucial procedural techniques needed to accomplish highly reproducable and cost effective immunoprecipitations. The final optimization step verified the entire process and resulted in a better understanding of the total amount of antibodies needed to measure changes in the SUMO1 protein profile. Future projects will benefit by using this standardized protocol to accurately measure changes in the SUMO1 profile though mass spectromety and discern how the proteins differentially modified by SUMO1 correspond to networks of cellular pathways involved in specific mechanisms.

Chapter 4: Final conclusions and future directions

Changes in steady state transcript levels of SUMO1 measured by RT-qPCR gathered from the experiments conducted for this project fall in line with previously reported data and appear to have little to fluctuation after stress is induced. Neither RNA synthesis nor degradation is measured in this experiment but may also affect the total protein levels without being measurable itself by RT-qPCR. Another potential cause of the discrepancy seen between transcript levels and total protein may be in part due to changes in the translational activity of transcripts rather than the total copy number. This is an interesting and under investigated potential regulatory factor. The potential for polysomal translation to be occurring on a large fraction of transcripts will be the initial direction of future studies. The RNA from treated cells will be extracted and fractionated using a sucrose gradient. The percentage of transcripts with one ribosome will be distinguishable from the polysomal fraction containing multiple ribosomes per transcript.

Substrate targeting may also be a major factor involved with the regulation of SUMO1 as a cellular anti-viral and stress response. To address these interactions as potential regulatory factors involved in the cellular anti-viral response, future projects will utilize mass spectrometry to analyze anti-SUMO1 immunoprecipitation products after inducing cellular stress. The differentially modified proteins will be sub categorized by the functions to which they are commonly associated. Further investigation of these interactions will dictate the direction of focus.

Further studies are required to determine the relevance of the stress induced changes taking place at both the translational level as well as the SUMO1 substrate targeting level. The quality control and procedural techniques described herein will facilitate more accurate and reproducible results for future projects.

References:

1. Antos, J. M., Truttmann, M. C., & Ploegh, H. L. (2016). Recent advances in sortase-catalyzed ligation methodology. Current Opinion in Structural Biology, 38, 111-118. doi:10.1016/j.sbi.2016.05.021.
2. Barysch, S. V., Dittner, C., Flotho, A., Becker, J., & Melchior, F. (2014). Identification and analysis of endogenous SUMO1 and SUMO2/3 targets in mammalian cells and tissues using monoclonal antibodies. Nat Protoc Nature Protocols, 9(4), 896-909. doi:10.1038/nprot.2014.053.
3. Becker, J., Barysch, S. V., Karaca, S., Dittner, C., Hsiao, H., Diaz, M. B., . . . Melchior, F. (2013). Detecting endogenous SUMO targets in mammalian cells and tissues. Nat Struct Mol Biol Nature Structural & Molecular Biology, 20(4), 525-531. doi:10.1038/nsmb.2526.
4. Bender, C., Hall, H., Huang, J., Klimov, A., Cox, N., Hay, A., . . . Subbarao, K. (1999). Characterization of the Surface Proteins of Influenza A (H5N1) Viruses Isolated from Humans in 1997–1998. Virology, 254(1), 115-123. doi:10.1006/viro.1998.9529.
5. Bouvier, N. M., & Palese, P. (2008). The biology of influenza viruses. Vaccine, 26(4), 49-53. doi:10.1016/j.vaccine.2008.07.039.
6. Chan, C., Chu, H., Zhang, A. J., Leung, L., Sze, K., Kao, R. Y., . . . Yuen, K. (2016). Hemagglutinin of influenza A virus binds specifically to cell surface nucleolin and plays a role in virus internalization. Virology, 494, 78-88. doi:10.1016/j.virol.2016.04.008.
7. Chen, C., X. Zhuang. (2008). Epsin 1 is a cargo-specific adaptor for the clathrin-mediated endocytosis of the influenza virus. Proc. Natl. Acad. Sci. USA. 105:11790–11795. doi:10.1073/pnas.0803711105.
8. Chen, Z., & Krug, R. M. (2000). Selective nuclear export of viral mRNAs in influenza-virus-infected cells. Trends in Microbiology, 8(8), 376-383. doi:10.1016/s0966-842x(00)01794-7.

9. Chlanda, P., & Zimmerberg, J. (2016). Protein-lipid interactions critical to replication of the influenza A virus during infection. FEBS Lett F, 1-15. doi:10.1002/1873-3468.12118.
10. Cinti, S. (2005). Pandemic Influenza: Are We Ready? Disaster Management & Response, 3, 61-67. doi:10.1016/j.dmr.2005.05.002.
11. Cohen, S., Au, S., & Panté, N. (2011). How viruses access the nucleus. Biochimica Et Biophysica Acta, 1813(9), 1634-1645. doi:10.1016/j.bbamcr.2010.12.009.
12. Compans, R. W., Content, J., & Duesberg, P. H. (1972). Structure of the Ribonucleoprotein of Influenza Virus. Journal of Virology, 10(4), 795-800.
13. Cross, K., Langley, W., Russell, R., Skehel, J., & Steinhauer, D. (2009). Composition and Functions of the Influenza Fusion Peptide. Protein & Peptide Letters PPL, 16(7), 766-778. doi:10.2174/092986609788681715.
14. Das, K., Aramini, J. M., Ma, L.-C., Krug, R. M., & Arnold, E. (2010). Structures of influenza A proteins and insights into antiviral drug targets. Nature Structural & Molecular Biology, 17(5), 530–538. http://doi.org/10.1038/nsmb.1779.
15. Davis, A. S., Chertow, D. S., Kindrachuk, J., Qi, L., Schwartzman, L. M., Suzich, J., . . . Taubenberger, J. K. (2016). 1918 Influenza receptor binding domain variants bind and replicate in primary human airway cells regardless of receptor specificity. Virology, 493, 238-246. doi:10.1016/j.virol.2016.03.025.
16. Dias, A., Bouvier, D., Crépin, T., Mccarthy, A. A., Hart, D. J., Baudin, F., . . . Ruigrok, R. W. (2009). The cap-snatching endonuclease of influenza virus polymerase resides in the PA subunit. Nature, 458(7240), 914-918. doi:10.1038/nature07745.
17. Domingues, P., Golebiowski, F., Tatham, M., Lopes, A., Taggart, A., Hay, R., & Hale, B. (2015). Global Reprogramming of Host SUMOylation during Influenza Virus Infection. Cell Reports, 13(7), 1467-1480. doi:10.1016/j.celrep.2015.10.001
18. Drag, M., Mikolajczyk, J., Krishnakumar, I., Huang, Z., & Salvesen, G. (2008). Activity profiling of human deSUMOylating enzymes (SENPs) with synthetic substrates suggests

an unexpected specificity of two newly characterized members of the family. Biochem. J. Biochemical Journal, 409(2), 461-469. doi:10.1042/bj20070940.

19. Dudek, S.E., L. Wixler, C. Nordhoff, A. Nordmann, D. Anhlan, V. Wixler, and S. Ludwig (2011) The influenza virus PB1-F2 protein has interferon antagonistic activity. Biol Chem. 392(12): 1135-44.
20. Edinger, T. O., Pohl, M. O., Yángüez, E., & Stertz, S. (2015). Cathepsin W Is Required for Escape of Influenza A Virus from Late Endosomes. MBio, 6(3). doi:10.1128/mbio.00297-15.
21. Ehrhardt, C., Seyer, R., Hrincius, E. R., Eierhoff, T., Wolff, T., & Ludwig, S. (2010). Interplay between influenza A virus and the innate immune signaling. Microbes and Infection, 12(1), 81-87. doi:10.1016/j.micinf.2009.09.007.
22. Everett, R. D., Boutell, C., & Hale, B. G. (2013). Interplay between viruses and host sumoylation pathways. Nature Reviews Microbiology Nat Rev Micro, 11(6), 400-411. doi:10.1038/nrmicro3015.
23. Fodor, E. (2013). The RNA polymerase of influenza A virus: Mechanisms of viral transcription and replication. Av Acta Virologica, 57(02), 113-122. doi:10.4149/av_2013_02_113.
24. Forbes, N., Selman, M., Pelchat, M., Jia, J. J., Stintzi, A., & Brown, E. G. (2013). Identification of Adaptive Mutations in the Influenza A Virus Non-Structural 1 Gene That Increase Cytoplasmic Localization and Differentially Regulate Host Gene Expression. PLoS ONE, 8(12). doi:10.1371/journal.pone.0084673.
25. Fournier, E., Moules, V., Essere, B., Paillart, J., Sirbat, J., Cavalier, A., . . . Marquet, R. (2012). Interaction network linking the human H3N2 influenza A virus genomic RNA segments. Vaccine, 30(51), 7359-7367. doi:10.1016/j.vaccine.2012.09.079.
26. Galloway, S. E., Reed, M. L., Russell, C. J., & Steinhauer, D. A. (2013). Influenza HA Subtypes Demonstrate Divergent Phenotypes for Cleavage Activation and pH of Fusion:

Implications for Host Range and Adaptation. PLoS Pathogens, 9(2). doi:10.1371/journal.ppat.1003151.

27. Gamblin, S. J., & Skehel, J. J. (2010). Influenza Hemagglutinin and Neuraminidase Membrane Glycoproteins. Journal of Biological Chemistry, 285(37), 28403-28409. doi:10.1074/jbc.r110.129809
28. Gareau, J. R., & Lima, C. D. (2010). The SUMO pathway: Emerging mechanisms that shape specificity, conjugation and recognition. Nature Reviews Molecular Cell Biology Nat Rev Mol Cell Biol, 11(12), 861-871. doi:10.1038/nrm3011.
29. Golebiowski, F., Matic, I., Tatham, M. H., Cole, C., Yin, Y., Nakamura, A., . . . Hay, R. T. (2009). System-Wide Changes to SUMO Modifications in Response to Heat Shock. Science Signaling, 2(72). doi:10.1126/scisignal.2000282.
30. Greco, A., Arata, L., Soler, E., Gaume, X., Coute, Y., Hacot, S., Calle, A., Monier, K., Epstein, A.L., Sanchez, J.C., Bouvet, P., Diaz, J.J., 2012. Nucleolin interacts with US11 protein of herpes simplex virus 1 and is involved in its trafficking. J. Virol. 86, 1449–1457.
31. Grove, J., & Marsh, M. (2011). The cell biology of receptor-mediated virus entry. The Journal of Cell Biology, 195(7), 1071-1082. doi:10.1083/jcb.201108131.
32. Hale BG, Randall RE, Ortin J, Jackson D (2008). The multifunctional NS1 protein of influenza A viruses. The Journal of general virology 89: 2359–2376.
33. Han, Q., Chang, C., Li, L., Klenk, C., Cheng, J., Chen, Y., . . . Xu, K. (2014). Sumoylation of Influenza A Virus Nucleoprotein Is Essential for Intracellular Trafficking and Virus Growth. Journal of Virology, 88(16), 9379-9390. doi:10.1128/jvi.00509-14
34. Hannoun, Z., Maarifi, G., & Chelbi-Alix, M. K. (2016). The implication of SUMO in intrinsic and innate immunity. Cytokine & Growth Factor Reviews. doi:10.1016/j.cytogfr.2016.04.003.
35. Hay, R. T. (2005). SUMO: a history of modification. Molecular Cell 18, 1–12.

36. Hickey, C. M., Wilson, N. R., & Hochstrasser, M. (2012). Function and regulation of SUMO proteases. Nature Reviews. Molecular Cell Biology, 13(12), 755–66. http://doi.org/10.1038/nrm3478.
37. Hochstrasser, M. (2000). Biochemical Functions of Ubiquitin and Ubiquitin-like Protein Conjugation. Protein Degradation Series, 249-278. doi:10.1002/9783527619320.ch11a.
38. Horimoto, T., & Kawaoka, Y. (2005). Influenza: lessons from past pandemics, warnings from current incidents. Nature Reviews. Microbiology, 3(8), 591–600. http://doi.org/10.1038/nrmicro1208.
39. Hsieh, Y., Kuo, H., Chang, C., Naik, M. T., Liao, P., Ho, C., . . . Shih, H. (2013). Ubc9 acetylation modulates distinct SUMO target modification and hypoxia response. The EMBO Journal, 32(6), 791-804. doi:10.1038/emboj.2013.5.
40. Huang, S., Chen, J., Chen, Q., Wang, H., Yao, Y., Chen, J., & Chen, Z. (2012). A Second CRM1-Dependent Nuclear Export Signal in the Influenza A Virus NS2 Protein Contributes to the Nuclear Export of Viral Ribonucleoproteins. Journal of Virology, 87(2), 767-778. doi:10.1128/jvi.06519-11.
41. Hutchinson, E., Orr, O., Liu, S., Engelhardt, O., & Fodor, E. (2011). Characterization of the interaction between the influenza A virus polymerase subunit PB1 and the host nuclear import factor Ran-binding protein 5. Journal of General Virology, 92(8), 1859-1869. doi:10.1099/vir.0.032813-0.
42. Hutchinson, E., & Fodor, E. (2012). Nuclear import of the influenza A virus transcriptional machinery. Vaccine, 30(51), 7353-7358. doi:10.1016/j.vaccine.2012.04.085.
43. Ito T, Couceiro JN, Kelm S, Baum LG, Krauss S, Castrucci MR, Donatelli I, Kida H, Paulson JC, Webster RG, & Kawaoka Y (1998). Molecular basis for the generation in pigs of influenza A viruses with pandemic potential. Journal of Virology, 72, 7367-7373.
44. Johnson, E. S. (2004). Protein Modification By Sumo. Annual Review of Biochemistry, 73, 355-382. doi:10.1146/annurev.biochem.73.011303.074118.

45. Johnson, N. P. A. S., & Mueller, J. (2002). Updating the accounts: global mortality of the 1918-1920 “Spanish” Influenza Pandemic. Bulletin of the History of Medicine, 76(1), 105–115. http://doi.org/10.1353/bhm.2002.0022.

46. Kagey, M. H., Melhuish, T. A., & Wotton, D. (2003). The Polycomb Protein Pc2 Is a SUMO E3. Cell, 113(1), 127-137. doi:10.1016/s0092-8674(03)00159-4.

47. Kageyama, T., Fujisaki, S., Takashita, E., Xu, H., Yamada, S., Uchida, Y., … Tashiro, M. (2013). Genetic analysis of novel avian A(H7N9) influenza viruses isolated from patients in China, February to April 2013. Euro Surveillance : Bulletin Europ??en Sur Les Maladies Transmissibles = European Communicable Disease Bulletin, 18(15), 20453. http://doi.org/10.1093/cid/cit294.

48. Kapp, L. D., & Lorsch, J. R. (2004). Molecular Mechanics of Eukaryotic Translation. Annual Review of Biochemistry, 73, 657-704. doi:10.1146/annurev.biochem.73.030403.080419.

49. Kochs, G., Garcia-Sastre, A., & Martinez-Sobrido, L. (2007). Multiple Anti-Interferon Actions of the Influenza A Virus NS1 Protein. Journal of Virology, 81(13), 7011-7021. doi:10.1128/jvi.02581-06.

50. Krug, R.M., W. Yuan, D.L. Noah, and A.G. Latham (2003) Intracellular warfare between human influenza viruses and human cells: the roles of the viral NS1 protein. Virology. 309(2): 181-9.

51. Linden, R. V., Frenken, L., Geus, B. D., Harmsen, M., Ruuls, R., Stok, W., . . . Verrips, C. (1999). Comparison of physical chemical properties of llama VHH antibody fragments and mouse monoclonal antibodies. Biochimica Et Biophysica Acta (BBA) - Protein Structure and Molecular Enzymology, 1431(1), 37-46. doi:10.1016/s0167-4838(99)00030-8

52. Liu, X., Wang, Q., Chen, W., & Wang, C. (2013). Dynamic regulation of innate immunity by ubiquitin and ubiquitin-like proteins. Cytokine & Growth Factor Reviews, 24(6), 559-570. doi:10.1016/j.cytogfr.2013.07.002.

53. Luo, M. (2011). Influenza Virus Entry. Advances in Experimental Medicine and Biology, 726, 201-221. doi:10.1007/978-1-4614-0980-9_9.

54. Maines, T. R., Belser, J. A., Gustin, K. M., van Hoeven, N., Zeng, H., Svitek, N., … Tumpey, T. M. (2012). Local innate immune responses and influenza virus transmission and virulence in ferrets. The Journal of Infectious Diseases, 205(3), 474–485. http://doi.org/10.1093/infdis/jir768.

55. Matrosovich M, Tuzikov A, Bovin N, Gambaryan A, Klimov A, Castrucci MR, Donatelli I, & Kawaoka Y. (2000). Early alterations of the receptor-binding properties of H1, H2, and H3 avian influenza virus hemagglutinins after their introduction into mammals. Journal of Virology, 74, 8502-8512.

56. Matsuoka, Y., Matsumae, H., Katoh, M., Eisfeld, A. J., Neumann, G., Hase, T., . . . Kawaoka, Y. (2013). A comprehensive map of the influenza A virus replication cycle. BMC Systems Biology, 7(1), 97. doi:10.1186/1752-0509-7-97.

57. Meyer, T. D., Muyldermans, S., & Depicker, A. (2014). Nanobody-based products as research and diagnostic tools. Trends in Biotechnology, 32(5), 263-270. doi:10.1016/j.tibtech.2014.03.001.

58. Melchior, F., Schergaut, M., & Pichler, A. (2003). SUMO: Ligases, isopeptidases and nuclear pores. Trends in Biochemical Sciences, 28(11), 612-618. doi:10.1016/j.tibs.2003.09.002.

59. Mercer J. & Helenius A., (2012). Gulping rather than sipping: Macropinocytosis as a way of virus entry. Current Opinion in Microbiology, 15(4), 490-499. doi:10.1016/j.mib.2012.05.016.

60. Min, J., & Krug, R. M. (2006). The primary function of RNA binding by the influenza A virus NS1 protein in infected cells: Inhibiting the 2'-5' oligo (A) synthetase/RNase L pathway. Proceedings of the National Academy of Sciences, 103(18), 7100-7105. doi:10.1073/pnas.0602184103.

61. Mok, B. W., Song, W., Wang, P., Tai, H., Chen, Y., Zheng, M., . . . Chen, H. (2012). The NS1 Protein of Influenza A Virus Interacts with Cellular Processing Bodies and Stress Granules through RNA-Associated Protein 55 (RAP55) during Virus Infection. Journal of Virology, 86(23), 12695-12707. doi:10.1128/jvi.00647-12
62. Moore, K. A., Plant, J. J., Gaddam, D., Craft, J., & Hollien, J. (2013). Regulation of Sumo mRNA during Endoplasmic Reticulum Stress. PLoS ONE, 8(9). doi:10.1371/journal.pone.0075723.
63. Mubareka, S., Lowen, A. C., Steel, J., Coates, A., Garcia-Sastre, A., & Palese, P. (2013). Transmission of Infleunza Virus via Aerosols and Fomites in the Guinea Pig Model. J Infect Dis, 18(9), 1199–1216. http://doi.org/10.1016/j.micinf.2011.07.011.
64. Naffakh, N., Tomoiu, A., Rameix-Welti, M., & Werf, S. V. (2008). Host Restriction of Avian Influenza Viruses at the Level of the Ribonucleoproteins. Annual Review of Microbiology Annu. Rev. Microbiol., 62(1), 403-424. doi:10.1146/annurev.micro.62.081307.162746.
65. Nayak, D. P., Balogun, R. A., Yamada, H., Zhou, Z. H., & Barman, S. (2009). Influenza virus morphogenesis and budding. Virus Research, 143(2), 147-161. doi:10.1016/j.virusres.2009.05.010.
66. Nelson, M. I., & Vincent, A. L. (2015). Reverse zoonosis of influenza to swine: New perspectives on the human–animal interface. Trends in Microbiology, 23(3), 142-153. doi:10.1016/j.tim.2014.12.002.
67. Neumann, G. (2000). Influenza A virus NS2 protein mediates vRNP nuclear export through NES-independent interaction with hCRM1. The EMBO Journal, 19(24), 6751-6758. doi:10.1093/emboj/19.24.6751.
68. Novel Swine-Origin Influenza A (H1N1) Virus Investigation Team, Dawood FS, Jain S, Finelli L, Shaw MW, Lindstrom S, et al. Emergence of a novel swine-origin influenza A (H1N1) virus in humans. N Engl J Med 2009;360:2605-15.

69. Octaviani, C. P., Ozawa, M., Yamada, S., Goto, H., & Kawaoka, Y. (2010). High Level of Genetic Compatibility between Swine-Origin H1N1 and Highly Pathogenic Avian H5N1 Influenza Viruses. J. Virol. Journal of Virology, 84(20), 10918-10922. doi:10.1128/jvi.01140-10

70. O'Neill, R. E., Jaskunas, R., Blobel, G., Palese, P. & Moroianu, J. (1995). Nuclear import of influenza virus RNA can be mediated by viral nucleoprotein and transport factors required for protein import. Journal of Biol Chem 270, 22701–22704.

71. Pal, S., Rosas, J. M., & Rosas-Acosta, G. (2010). Identification of the non-structural influenza A viral protein NS1A as a bona fide target of the Small Ubiquitin-like MOdifier by the use of dicistronic expression constructs. Journal of Virological Methods, 163(2), 498-504. doi:10.1016/j.jviromet.2009.11.010

72. Pal, S., Santos, A., Rosas, J. M., Ortiz-Guzman, J., & Rosas-Acosta, G. (2011). Influenza A virus interacts extensively with the cellular SUMOylation system during infection. Virus Research, 158(1-2), 12-27. doi:10.1016/j.virusres.2011.02.017

73. Palese, P. and M.L. Shaw (2007) Orthomyxoviridae: The viruses and their replication. In: Fields' Virology. D.M. Knipe and P.M. Howley, Editors. Lippincott Williams & Wilkins: Philadelphia. p. 1647-1689.

74. Pillet, S., Kobasa, D., Meunier, I., Gray, M., Laddy, D., Weiner, D. B., … Kobinger, G. P. (2011). Cellular immune response in the presence of protective antibody levels correlates with protection against 1918 influenza in ferrets. Vaccine, 29(39), 6793–6801. http://doi.org/10.1016/j.vaccine.2010.12.059.

75. Portela, A., & Digard, P. (2002). The influenza virus nucleoprotein: A multifunctional RNA-binding protein pivotal to virus replication. Journal of General Virology, 83(4), 723-734. doi:10.1099/0022-1317-83-4-723.

76. Randall, R. E., & Goodbourn, S. (2008). Interferons and viruses: An interplay between induction, signalling, antiviral responses and virus countermeasures. Journal of General Virology, 89(1), 1-47. doi:10.1099/vir.0.83391-0.
77. Rao, S., Zang, X., Yang, Z., Gao, L., Yin, Y., & Fang, W. (2016). Soluble expression and purification of the recombinant bioactive peptide precursor BPP-1 in Escherichia coli using a cELP-SUMO dual fusion system. Protein Expression and Purification, 118, 113-119. doi:10.1016/j.pep.2015.11.005
78. Rewar, S., Mirdha, D., & Rewar, P. (2015). Treatment and Prevention of Pandemic H1N1 In fl uenza. Annals of Global Health, 81(5). http://doi.org/10.1016/j.aogh.2015.08.014
79. Rodriguez, M. S., Dargemont, C., & Hay, R. T. (2000). SUMO-1 Conjugation in Vivo Requires Both a Consensus Modification Motif and Nuclear Targeting. Journal of Biological Chemistry, 276(16), 12654-12659. doi:10.1074/jbc.m009476200.
80. Rosas-Acosta, G., Russell, W. K., Deyrieux, A., Russell, D. H., & Wilson, V. G. (2005). A Universal Strategy for Proteomic Studies of SUMO and Other Ubiquitin-like Modifiers. Molecular & Cellular Proteomics, 4(1), 56-72. doi:10.1074/mcp.m400149-mcp200
81. Rossman, J. S., Jing, X., Leser, G. P., & Lamb, R. A. (2010). Influenza Virus M2 Protein Mediates ESCRT-Independent Membrane Scission. Cell, 142(6), 902-913. doi:10.1016/j.cell.2010.08.029
82. Rossman, J. S., & Lamb, R. A. (2011). Influenza virus assembly and budding. Virology, 411(2), 229-236. doi:10.1016/j.virol.2010.12.003
83. Sahin, U., Ferhi, O., Carnec, X., Zamborlini, A., Peres, L., Jollivet, F., . . . Lallemand-Breitenbach, V. (2014). Interferon controls SUMO availability via the Lin28 and let-7 axis to impede virus replication. Nature Communications Nat Comms, 5. doi:10.1038/ncomms5187.
84. Santos, A., Pal, S., Chacon, J., Meraz, K., Gonzalez, J., Prieto, K., & Rosas-Acosta, G. (2013). SUMOylation Affects the Interferon Blocking Activity of the Influenza A

Nonstructural Protein NS1 without Affecting Its Stability or Cellular Localization. Journal of Virology, 87(10), 5602-5620. doi:10.1128/jvi.02063-12.

85. Scull, M. A., & Rice, C. M. (2010). A big role for small RNAs in influenza virus replication. Proceedings of the National Academy of Sciences, 107(25), 11153-11154. doi:10.1073/pnas.1006673107.

86. Steinhauer, D. A., & Skehel, J. J. (2002). Genetics of influenza viruses. Annual Review of Genetics, 36, 305-332. doi:10.1146/annurev.genet.36.052402.152757.

87. Tang, Y., Zhong, G., Zhu, L., Liu, X., Shan, Y., Feng, H., . . . Wang, C. (2010). Herc5 Attenuates Influenza A Virus by Catalyzing ISGylation of Viral NS1 Protein. The Journal of Immunology, 184(10), 5777-5790. doi:10.4049/jimmunol.0903588

88. Tao, H., Li, L., White, M. C., Steel, J., & Lowen, A. C. (2015). Influenza A Virus Coinfection through Transmission Can Support High Levels of Reassortment. Journal of Virology, 89(16), 8453–8461. http://doi.org/10.1128/JVI.01162-15.

89. Tatham, M. H., Jaffray, E., Vaughan, O. A., Desterro, J. M., Botting, C. H., Naismith, J. H., & Hay, R. T. (2001). Polymeric Chains of SUMO-2 and SUMO-3 Are Conjugated to Protein Substrates by SAE1/SAE2 and Ubc9. Journal of Biological Chemistry, 276(38), 35368-35374. doi:10.1074/jbc.m104214200

90. Tawaratsumida, K., Phan, V., Hrincius, E. R., High, A. A., Webby, R., Redecke, V., & Hacker, H. (2014). Quantitative Proteomic Analysis of the Influenza A Virus Nonstructural Proteins NS1 and NS2 during Natural Cell Infection Identifies PACT as an NS1 Target Protein and Antiviral Host Factor. Journal of Virology, 88(16), 9038-9048. doi:10.1128/jvi.00830-14.

91. Tayyari, F., Marchant, D., Moraes, T.J., Duan, W., Mastrangelo, P., Hegele, R.G., 2011. Identification of nucleolin as a cellular receptor for human respiratory syncytial virus. Nat. Med. 17, 1132–1135.

92. Schmittgen, T. D., & Zakrajsek, B. A. (2000). Effect of experimental treatment on housekeeping gene expression: Validation by real-time, quantitative RT-PCR. Journal of Biochemical and Biophysical Methods, 46(1-2), 69-81. doi:10.1016/s0165-022x(00)00129-9

93. Thompson, W. W., Shay, D. K., Weintraub, E., Brammer, L., Cox, N., Anderson, L. J., & Fukuda, K. (2003). Mortality Associated with Influenza and Respiratory Syncytial Virus in the United States. American Medical Association, 289(2), 179–186.

94. Thompson, W. W., Shay, D. K., Weintraub, E., Brammer, L., Cox, N., Bridges, C. B., & Fukuda, K. (2004). Influenza-Associated Hospitalizations in the United States, 292(3), 1333–1340.

95. Tong, S., Li, Y., Rivailler, P., Conrardy, C., Castillo, D. A., Chen, L., . . . Donis, R. O. (2012). A distinct lineage of influenza A virus from bats. Proceedings of the National Academy of Sciences, 109(11), 4269-4274. doi:10.1073/pnas.1116200109.

96. Tong, S., Zhu, X., Li, Y., Shi, M., Zhang, J., Bourgeois, M., . . . Donis, R. O. (2013). New World Bats Harbor Diverse Influenza A Viruses. PLoS Pathog PLoS Pathogens, 9(10). doi:10.1371/journal.ppat.1003657.

97. Ulmanen, I., Broni, B. A., & Krug, R. M. (1981). Role of two of the influenza virus core P proteins in recognizing cap 1 structures (m7GpppNm) on RNAs and in initiating viral RNA transcription. Proceedings of the National Academy of Sciences, 78(12), 7355-7359. doi:10.1073/pnas.78.12.7355.

98. Wang, Y., & Dasso, M. (2009). SUMOylation and deSUMOylation at a glance. Journal of Cell Science, 122(23), 4249-4252. doi:10.1242/jcs.050542.

99. Watanabe, T., Watanabe, S., & Kawaoka, Y. (2010). Cellular Networks Involved in the Influenza Virus Life Cycle. Cell Host & Microbe, 7(6), 427-439. doi:10.1016/j.chom.2010.05.008.

100. White, J. M., & Whittaker, G. R. (2016). Fusion of Enveloped Viruses in Endosomes. Traffic, 1-22. doi:10.1111/tra.12389.

101. Worch, R. (2014). Structural biology of the influenza virus fusion peptide. Acta Biochim Polonica, 61(3), 421-426.

102. World Health Organization. Pandemic (H1N1) 2009: update 112 [Internet]. Geneva: World Health Organization; 2010 [cited 2010 Oct 4]. Available from: http://www.who.int/csr/don/2010_08_06/en/index.html.

103. Wu, C., Jeng, K., & Lai, M. M. (2011). The SUMOylation of Matrix Protein M1 Modulates the Assembly and Morphogenesis of Influenza A Virus. Journal of Virology, 85(13), 6618-6628. doi:10.1128/jvi.02401-10

104. Wu, W. W., Sun, Y. B., & Pante, N. (2007). Nuclear import of influenza A viral ribonucleoprotein complexes is mediated by two nuclear localization sequences on viral nucleoprotein. Virology Journal Virol J, 4(1), 49. doi:10.1186/1743-422x-4-49.

105. Ye, Q., Krug, R. M., & Tao, Y. J. (2006). The mechanism by which influenza A virus nucleoprotein forms oligomers and binds RNA. Nature, 444(7122), 1078-1082. doi:10.1038/nature05379.

106. Yuan, P., Bartlam, M., Lou, Z., Chen, S., Zhou, J., He, X., . . . Liu, Y. (2009). Crystal structure of an avian influenza polymerase PAN reveals an endonuclease active site. Nature, 458(7240), 909-913. doi:10.1038/nature07720.

107. Xu, K., Klenk, C., Liu, B., Keiner, B., Cheng, J., Zheng, B., . . . Sun, B. (2010). Modification of Nonstructural Protein 1 of Influenza A Virus by SUMO1. Journal of Virology, 85(2), 1086-1098. doi:10.1128/jvi.00877-10.

Vita

David Quintanar graduated from Americas High School, El Paso, Texas in the spring of 2003 and since has pursued multiple goals across several different fields. In 2005, he entered a culinary program and by 2007 was promoted to sous chef of an El Paso Italian restaurant. He continued working as a chef and restaurant manager until 2013 when he re-enrolled as an undergraduate at The University of Texas at El Paso. While pursuing a bachelor's degree in biology, he was selected to be a Research Initiative for Science Enhancement (RISE) scholar. During the summer of 2013, he worked as an undergraduate research assistant in the SUMO/Influenza laboratory directed by Dr. German Rosas-Acosta. During this time, David discovered his passion for science and education.

To continue in academia, David entered the graduate program in pathobiology at the same university and was awarded the education centered Graduate K-12 fellowship (GK-12) for two years. This program placed real scientists into high school classrooms and taught us how to develop high impact project based activities; this pedagogical technique is designed to enhance student interest and overall retention. During this time, he continued to investigate interactions taking place between the host SUMOylation system and the influenza A virus. He put into place several novel protocols utilizing new and unique techniques which are still in place today. The use of hybridoma technology to synthesize monoclonal antibodies was pioneered at The University of Texas at El Paso by David and will be used in the future to efficiently culture antibodies. He will be a co-author on two papers to be submitted soon. After graduation, he plans to contribute to the field of science by creating new STEAM based programs for early childhood education.

This thesis was typed by David Quintanar